NACA

RESEARCH MEMORANDUM

INVESTIGATION AT LOW SPEED OF THE FLOW FIELD BEHIND THE

LIFTING SURFACES OF A MODEL EQUIPPED WITH A

60° TRIANGULAR WING AND A 60° TRIANGULAR

CANARD TAIL

By Ernest E. Newman and Jones F. Cahill

Langley Aeronautical Laboratory
Langley Field, Va.

TECH. LIBRARY
AFL 2611

CLASSIFIED DOCUMENT

This material contains information affecting the National Defense of the United States within the meaning of the espionage laws, Title 18, U.S.C., Secs. 793 and 794, the transmission or revelation of which in any manner to an unauthorized person is prohibited by law.

NATIONAL ADVISORY COMMITTEE
FOR AERONAUTICS

WASHINGTON
June 29, 1953

N

JUN 1 6 1983

139A

TO: Distribution

FROM: 180A/Security Classification Officer

SUBJECT: Authority to Declassify NACA/NASA Documents Dated Prior to
         January 1, 1960

(informal, correspondence)

Effective this date, all material classified by this Center prior to
January 1, 1960, is declassified. This action does not include material
derivatively classified at the Center upon instructions from other Agencies.

Immediate re-marking is not required; however, until material is re-marked by
lining through the classification and annotating with the following statement,
it must continue to be protected as if classified:

    "Declassified by authority of LaRC Security Classification Officer (SCO)
    letter dated June 16, 1983," and the signature of person performing the
    re-marking.

If re-marking a large amount of material is desirable, but unduly burdensome,
custodians may follow the instructions contained in NHB 1640.4, subpart F,
section 1203.604, paragraph (h).

This declassification action complements earlier actions by the National
Archives and Records Service (NARS) and by the NASA Security Classification
Officer (SCO). In Declassification Review Program 807008, NARS declassified
the Center's "Research Authorization" files, which contain reports, Research
Authorizations, correspondence, photographs, and other documentation.
Earlier, in a 1971 letter, the NASA SCO declassified all NACA/NASA formal
series documents with the exception of the following reports, which must
remain classified:

Document No.	First Author
E-51A30	Nagey
E-53G20	Francisco
E-53G21	Johnson
E-53K18	Spooner
SL-54J21a	Westphal
E-55C16	Fox
E-56H23a	Himmel
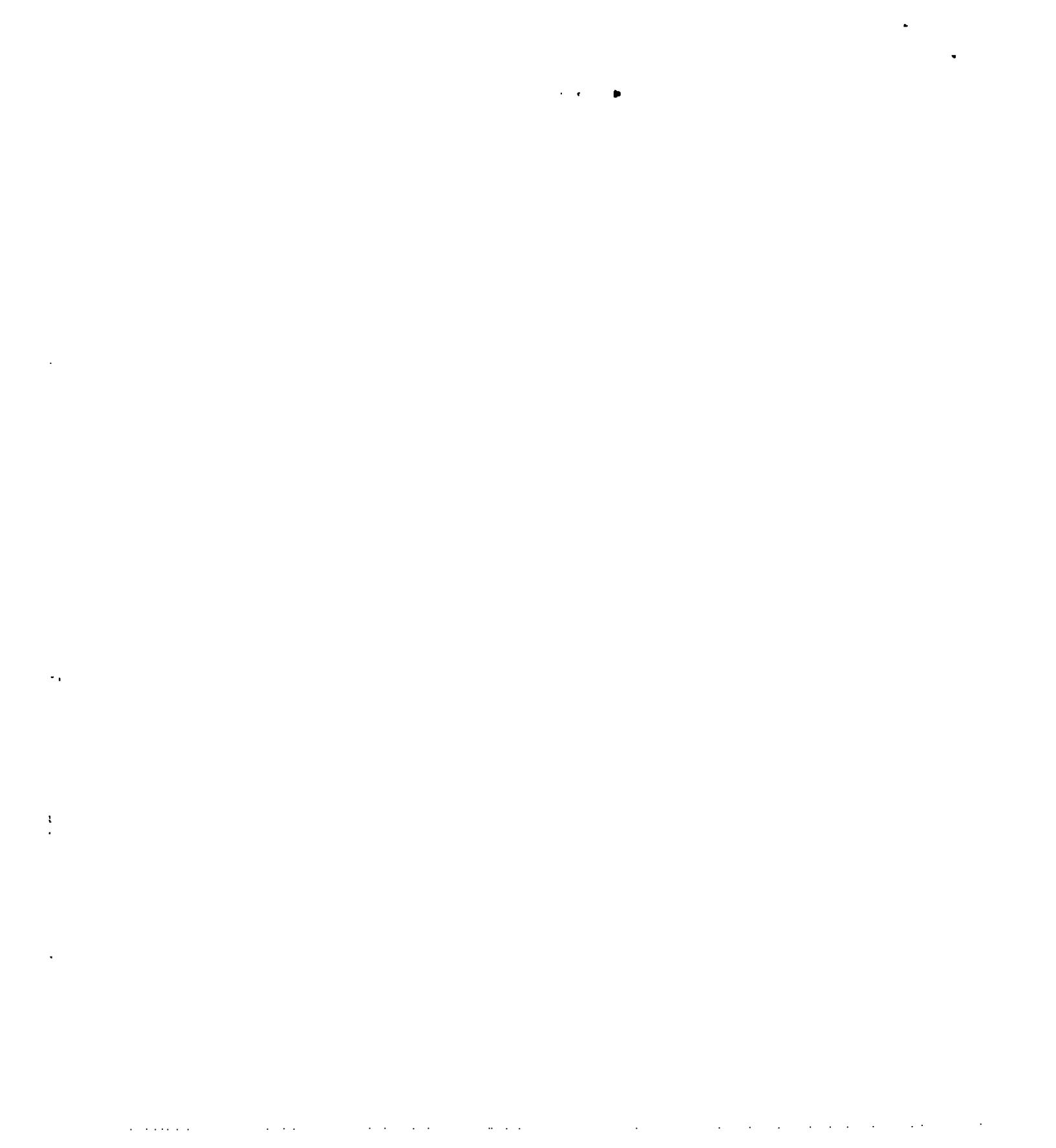
JUN 2 1 1983
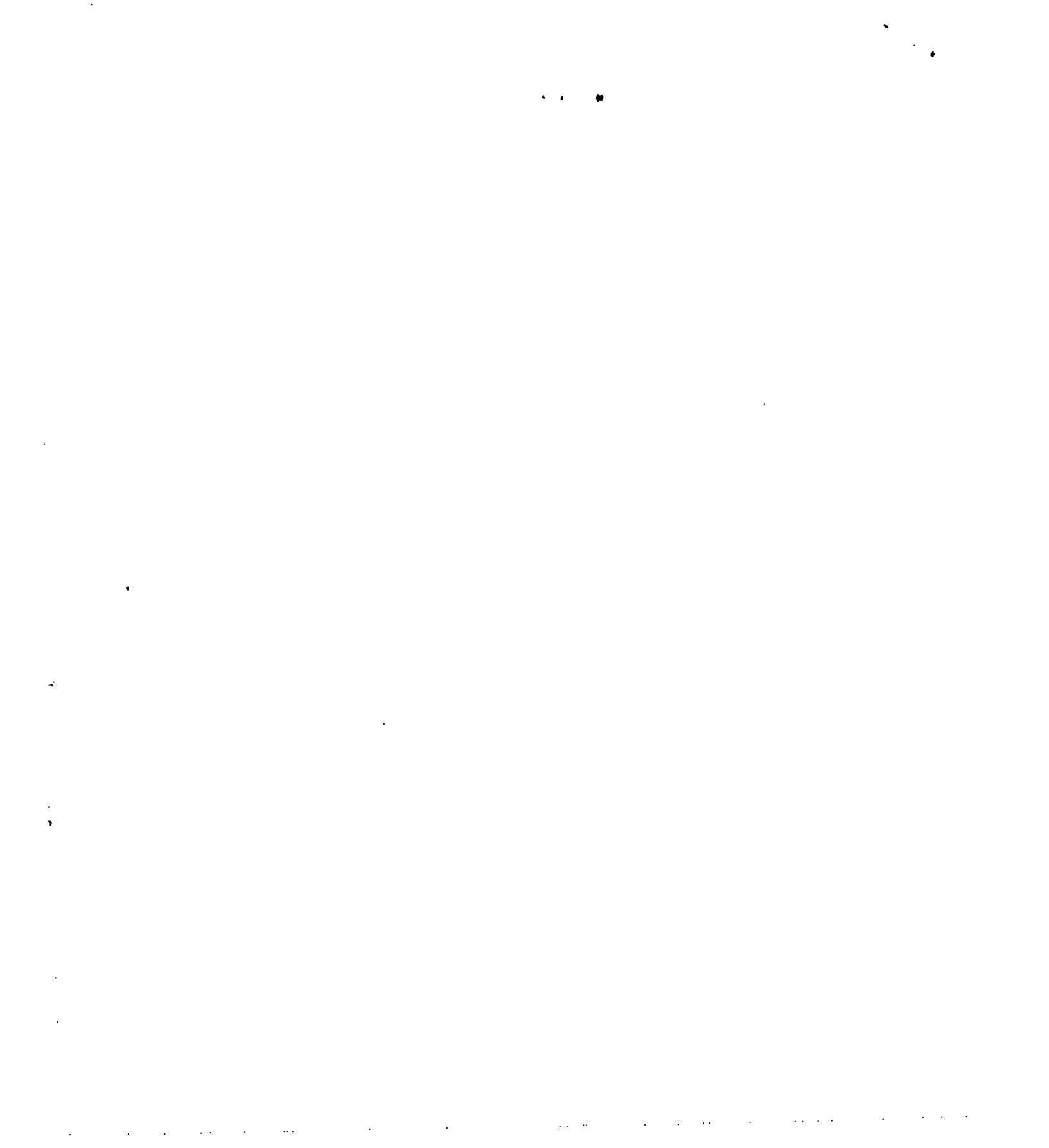
NATIONAL ADVISORY COMMITTEE FOR AERONAUTICS

RESEARCH MEMORANDUM

INVESTIGATION AT LOW SPEED OF THE FLOW FIELD BEHIND THE

LIFTING SURFACES OF A MODEL EQUIPPED WITH A

60° TRIANGULAR WING AND A 60° TRIANGULAR

CANARD TAIL

By Ernest E. Newman and Jones F. Cahill

SUMMARY

An investigation was made at a Mach number of 0.14 and a Reynolds number of 9×10^6 of the flow field behind the lifting surfaces of a model equipped with a 60° triangular wing and a 60° triangular canard tail. Downwash, sidewash, and dynamic-pressure measurements were made at two longitudinal locations behind the wing with the canard tail removed, behind the tail at the location of the leading edge of the wing mean aerodynamic chord (wing removed), and 0.25 mean aerodynamic chord ahead of the wing trailing edge (wing in place).

The data obtained showed that the effective downwash behind 60° triangular wings experiencing vortex flow is a certain function of lift coefficient regardless of differences in wing configuration or test conditions which cause rather large changes in lift curves. Analysis of flow data shows that, for the rear tail locations investigated, increases in tail area, aspect ratio, or taper ratio would, in general, produce an increase in the tail-effectiveness factor $\left(1 - \dfrac{d\epsilon}{d\alpha}\right)\left(\dfrac{q_t}{q}\right)_e$. At high angles of attack, the inboard movement of the separation vortex would cause large interference effects on vertical tails located either centrally or outboard on the wing. The flow field behind the canard tail at zero deflection would have little effect on the flow over the wing.

INTRODUCTION

The use of wings having low aspect ratios and high sweep angles has introduced serious problems in relation to the effectiveness of tail surfaces on high-speed airplanes. Several investigations at rather low Reynolds numbers (ref. 1, for example) have shown that the flow

at probable rear tail locations is characterized by high values of and large gradients in both sidewash and downwash as a result of regions of high vorticity which usually accompany leading-edge separation on highly swept wings. These effects may be significant in the flow field behind any low-aspect-ratio lifting surface whether used as a wing or, for example, as a canard control surface.

The present paper presents the results of an investigation in the Langley low-turbulence pressure tunnel at a fairly high Reynolds number of the flow field in several longitudinally located planes for a 60° triangular wing and canard tail mounted separately and in combination on a fuselage. Downwash, sidewash, and dynamic pressures were measured in planes at two longitudinal locations (0.5 mean aerodynamic chord and 1.0 mean aerodynamic chord) behind the trailing edge of the wing mounted on a fuselage with the canard tail off. With a small 60° tri-angular wing mounted as a canard tail, surveys were made at the location of the leading edge of the wing mean aerodynamic chord (wing removed) and 0.25 mean aerodynamic chord ahead of the wing trailing edge (wing in place). All flow surveys were made at a Mach number of 0.14 and a Reynolds number of 9×10^6. Some analysis is made of the effects of these flow patterns on the characteristics of the wing and of the rear tail surfaces.

SYMBOLS

Forces and moments presented in this paper are referred to the body axis which is illustrated in figure 1.

C_L lift coefficient, L/qS

C_D drag coefficient, D/qS

C_m pitching-moment coefficient, $M/qS\bar{c}$

L lift, lb

D drag, lb

M pitching moment about fuselage station 20, ft-lb

A aspect ratio, b^2/S

b span, ft

S area, sq ft

c　　　　　　local chord measured parallel to plane of symmetry, ft

$\bar{c}$　　　　　mean aerodynamic chord, $\dfrac{2}{S}\displaystyle\int_0^{b/2} c^2\,dy$, ft

x　　　　　chordwise distance from wing quarter chord, ft

y　　　　　spanwise distance from plane of symmetry, ft

z　　　　　vertical distance from chord plane, ft

R　　　　　Reynolds number, $\rho V\bar{c}/\mu$

ρ　　　　　free-stream mass density, slugs/cu ft

V　　　　　free-stream velocity, ft/sec

μ　　　　　absolute viscosity

q　　　　　free-stream dynamic pressure, $\rho V^2/2$, lb/sq ft

q_t　　　　　local-stream dynamic pressure, lb/sq ft

α　　　　　angle of attack, deg

β　　　　　angle of sideslip, deg

ϵ　　　　　angle of downwash with respect to free-stream direction, positive when the flow is directed downward, deg

ϵ'　　　　　angle of downwash with respect to chord-plane extended, positive when the flow is directed downward, $\epsilon' \approx \epsilon - \alpha$, deg

σ　　　　　angle of sidewash with respect to free-stream direction, positive when flow is directed to left when viewed from rear, deg

σ'　　　　　angle of sidewash with respect to body axis, positive when flow is directed to left when viewed from rear, $\sigma' \approx \sigma + \beta$, deg

$(q_t/q)_e$　　　effective q_t/q, obtained by

$$(q_t/q)_e = \int_0^1 \frac{q_t}{q}\left(c/c_{av}\right)_t\, d\!\left(\frac{y}{b/2}\right)_t$$

ϵ_e effective ϵ, obtained by

$$\epsilon_e = \frac{1}{\left(q_t/q\right)_e} \int_0^1 \epsilon \, \frac{q_t}{q} \left(c/c_{av}\right)_t \, d\left(\frac{y}{b/2}\right)_t$$

c_t chord of tail, ft

b_t span of tail, ft

y_t .   spanwise distance, ft

$\left(c/c_{av}\right)_t$ ratio of local chord of tail to average chord of tail

δ_t canard-tail deflection, positive with leading edge up, deg

MODEL AND TESTS

Description of model.- A sketch of the model used for these tests, together with locations of flow-survey planes, are shown in figures 2 and 3 and photographs of the complete test setup are shown in figure 4. The basic model consisted of a 60° triangular wing having NACA 65A006 airfoil sections mounted on a body having a transonic drop body shape. The ratio of wing span to body diameter was 5.47 and the body fineness ratio was 10. Some tests were made with a canard horizontal tail to investigate the flow in the region of the wing as affected by the presence of the tail. The canard tail was of the same plan form and section as the wing, with an area equal to 20 percent of the wing area and the quarter-chord point of the tail was mounted 1.73$\bar{c}$ forward of the quarter-chord point of the wing mean aerodynamic chord. Pertinent dimensions of the model are shown in figure 2 and table I.

Scope of tests.- The lift, drag, and pitching-moment data for configurations B and C are presented in figures 5 and 6, respectively. All flow-survey results presented in the present paper were obtained at a Reynolds number of 9 × 10⁶ and a Mach number of 0.14 (figs. 7 to 15). Measurements of the local downwash, sidewash, and dynamic pressure were made for several angles of attack at two longitudinal stations behind the wing to determine the flow characteristics at possible rearward horizontal-tail locations. With the canard horizontal tail in place, surveys were made above and below the wing at a location 1/4$\bar{c}$ forward of the wing trailing edge at several yaw angles to determine the flow characteristics at possible locations of a vertical tail. In order to gain some insight into the effect of the canard horizontal tail on the flow at the wing, a survey was made behind the horizontal tail with the wing removed. The survey plane

for this test was placed at the location of the leading edge of the wing mean aerodynamic chord for the rear wing position. The locations of the planes in which the flow surveys were made and the model configurations appropriate to each are listed in the following table and illustrated in figure 3:

Location of survey plane, $\bar{c}$	Wing position	Canard horizontal tail	α, deg	β, deg	Figure number (flow-survey data)
0.5 behind wing trailing edge	Fore	Off	8.6, 17.2, 25.7, 33.9	0	7
1.0 behind wing trailing edge	Fore	Off	8.6, 17.2, 25.7, 33.9	0	8
0.25 forward of trailing edge	Rear	On	8.6, 25.7	0, $-3\frac{1}{2}$, -7	11-12
1.93 behind body nose	Off	On	8, 16, 24, 32	0	14

Test method.- Measurements of the local flow angularity and dynamic pressure were made with a rake of 10 spherical-nosed pitch, yaw, and static-pressure measuring tubes. Calibrations of the measuring rake were made by mounting the rake alone in the tunnel at various pitch and yaw angles. The accuracy of measurements made with tubes of this type is a function of the flow angularity and is poorest at the highest angles. Duplicate measurements obtained for several conditions during the calibrations of the survey tubes showed that, at the highest angles reported (approx. 40° with respect to the tube axis), the angles are reliable within about 1° and dynamic-pressure ratios within about 0.03. In cases where the stream angularity exceeded 40°, the data are not considered reliable and have been omitted from the figures. Forty tube locations were used for each survey plane (for a single semispan) behind the canard tail and fifty locations for survey planes behind the wing.

The survey rake was attached to the sting which supported the model and changed angle of attack with the model. Variations in the vertical position of the rake were obtained by shifting

the rake up and down along a rail mounted perpendicular to the sting axis. The survey planes are therefore oriented perpendicular to the wing-chord plane extended. All surveys were made behind one wing semi-span and the data shown in figures 11 and 12 for the full span with the model yawed were obtained by combining data measured at equal positive and negative sideslip angles. In cases where the data were faired through steep gradients at the model center line, the contours are shown as dashed lines to indicate some question as to the exact location of the contours.

Model lift, drag, and pitching-moment data were obtained from a six-component strain-gage balance mounted within the fuselage.

Corrections to data.- All pressure readings and the model force and moment coefficients were corrected for tunnel blocking effects by a method based on information presented in references 2 and 3. Corrections to angles of attack, downwash angles, and drag coefficients to account for the induced upwash produced by the jet boundaries have been determined by the method of reference 4. These corrections have been applied to all the angle-of-attack and drag-coefficient data. Downwash data presented in the contours of figures 7, 8, 11, 12, and 14 have not been corrected for this induced-upwash effect, but any downwash data presented in other figures have been corrected.

Due to the boundary-induced upwash effects, the flow field behind the model as measured in a closed-throat wind tunnel will be raised from the position it would assume in free air. This change in the vertical position of the flow field is usually small and has no great significance for normal types of wings. For wings of low aspect ratio or swept wings experiencing the separation-vortex type of flow, however, large gradients in flow angularity and dynamic pressure can exist at locations near the horizontal tail. In these cases, therefore, even small changes in the vertical position of the flow field can have a large effect on flow conditions at the tail. The corrections to vertical position (in fractions of semispan) which should apply to the data obtained are $0.0092C_L$ and $0.0196C_L$ for positions $0.5\bar{c}$ and $1.0\bar{c}$, respectively, behind the wing. This correction has not been applied to any of the data presented in this paper.

The effects of the presence of the sting support on forces measured in this test setup have been determined and applied to the data presented in this paper. This correction was found to be negligible for all the force components except drag for which an increment was found which varied from about 0.003 at zero lift to about 0.015 at the highest lift coefficients.

RESULTS AND DISCUSSION

Force and Moment Data

Lift, drag, and pitching-moment data for the wing-fuselage and wing-fuselage canard-tail configurations are shown in figures 5 and 6. The pitching moments were measured about an axis 20 inches behind the nose of the fuselage. For the data presented in figure 5, fuselage station 20 is coincident with the quarter-chord point of the mean aerodynamic chord; in figure 6, the wing was moved 3 inches (0.285$\bar{c}$) rearward relative to the fuselage.

No scale effect is indicated for lift coefficients below 0.2 (see fig. 5). At higher lift coefficients, increasing the Reynolds number causes decreases in drag and slight increases in lift and in the negative value of the pitching moment. These data show the high maximum lift coefficients and nearly constant center-of-pressure position which are characteristics of delta wings experiencing leading-edge separation. The increase in lift-curve slope, which is indicative of the formation of a strong separation-vortex type of flow, begins at a lift coefficient of about 0.4.

The pitching-moment data for the wing in the rear position (fig. 6) show an abrupt unstable change near maximum lift which was considerably alleviated by the addition of the canard tail. For the moment axes chosen for these tests, the static margin for the rear wing position with the canard tail is approximately the same as that for the wing alone in the forward position.

Air-Stream Surveys Behind the Wing

The air-stream-survey data are presented in the form of contour charts of downwash, sidewash, and dynamic-pressure ratio. Results of the survey for the two planes located at longitudinal distances of 0.5$\bar{c}$ and 1.0$\bar{c}$ behind the wing trailing edge are shown in figures 7 and 8, respectively. The angularity of flow for the downwash and sidewash contours is referenced to the body axis; that is, the downwash angle is referred to the chord plane extended and the sidewash angle is referred to the plane of symmetry. Because the contribution of the tail to the stability of an airplane is greatly affected by the local flow angularity, the behavior of the trailing-vortex sheet and the rolling up of the vortices are of utmost importance when considering possible rear tail locations. The development of the rolled-up vortices can be traced in the air-stream surveys by defining the vortex center to be at the intersection of the zero downwash and sidewash contours when the flow angles are referred to the free-stream direction. The data in figures 7 and 8 show

that this region is near the region of maximum reduction in the dynamic-pressure ratio. The coincidence of these two regions is poor for low lift coefficients at the 0.5$\bar{c}$ survey station and best for high lift coefficients at the rear survey station where the trailing-vortex system is more completely rolled up.

According to theory (ref. 5) the rates of rolling up of the vortex sheet behind wings having similar span loading vary directly with lift coefficient and inversely with aspect ratio so that the trailing vortex sheet behind low-aspect-ratio wings may become essentially rolled up into two trailing vortex cores within a short distance of the trailing edge. For a triangular wing with an aspect ratio of 2.31 and having elliptical span loading, theory predicts that the trailing vortex sheet will be essentially rolled up within 1 root chord at a lift coefficient of 0.7. The theory further predicts that the two vortex cores after leaving the wing tip will move inboard slightly at a rate depending on the lift coefficient but reaching a given asymptote when completely rolled up some place far down stream regardless of lift coefficient. Calculations of the development of the vortex sheet behind a low-aspect-ratio triangular wing (ref. 5) also show that the sheet rolls up into a pair of discrete vortices about a line which shows no vertical movement with respect to the air stream.

A study of the charts (figs. 7 and 8) shows that the motions of the trailing vortices are in good agreement with those predicted by theory. The vertical displacement of the vortex centers shown in figures 7 and 8 is primarily a result of the fact that the vertical position is measured from the chord plane extended and a consideration of the angle of attack of the chord plane shows that the vortex cores experience practically no vertical movement with respect to the free-stream direction. The span-wise position of the vortices moves inboard as the lift coefficient is increased; however, very little spanwise movement is indicated between the 0.5$\bar{c}$ and 1.0$\bar{c}$ survey stations for a lift coefficient of 0.79. This movement of the vortices in approximately parallel paths is an indication that a large part, but not necessarily all, of the rolling-up occurs upstream of the 0.5$\bar{c}$ measuring station. An analysis of the data in figures 7 and 8 also shows only a small change in vorticity near the plane of symmetry between the 0.5$\bar{c}$ and 1.0$\bar{c}$ survey stations, which is another indication that a large part of the rolling-up process is accomplished between the trailing edge of the wing and the 0.5$\bar{c}$ survey plane.

Effective Values of Downwash and Dynamic-Pressure Ratio

In order to evaluate the air-stream survey data at particular tail locations, the downwash angles and dynamic-pressure ratios have been weighted according to the chord of an assumed horizontal tail having the same plan form as the wing and an area equal to 25 percent of the

wing area and effective values determined by integrating these weighted values across the span of the horizontal tail assumed to be located at the positions of the survey planes. Integrations were performed at tail heights of 0.22b/2 above and below the chord plane, and one on the chord plane extended, for each of the two survey planes located at $0.5\bar{c}$ and $1.0\bar{c}$ behind the wing trailing edge.

These integrated values of downwash angle and dynamic-pressure ratio are presented in figure 9 and their combined effect on the stabilizing contribution of the horizontal tail is determined by use of the expression

$$\tau = \left(1 - \frac{d\epsilon_e}{d\alpha}\right)\left(\frac{q_t}{q}\right)_e$$

This expression will be referred to herein as the tail-effectiveness factor. The contribution of the horizontal tail to the stability of the configuration is directly proportional to the magnitude of this factor, positive values indicating an increase in stability.

Effect of Tail Height at $0.5\bar{c}$ Behind Wing Trailing Edge

Figure 9(a) shows that the horizontal tail should provide some contribution to the stability of the configuration at low angles of attack for all the tail positions considered. As the angle of attack is increased, however, the value of $d\epsilon_e/d\alpha$ increases and the tail in the two upper positions actually becomes destabilizing (the high tail location at an angle of attack of about 10° and the mid tail location at about 20°). The increase in $d\epsilon_e/d\alpha$ for the low tail position is rather small and the tail in this position should retain its effectiveness throughout the entire range of angle of attack.

A reference to figure 7 shows that the high downwash angles which result in undesirably high values of $d\epsilon_e/d\alpha$ for the high tail position are a result of the proximity of the tail to the centers of the trailing vortices. Another point of interest is that at angles of attack between 26° and 34° the downwash angles generally decrease as the wing stalls, resulting in large stabilizing contributions from the horizontal tail. This increase in the stabilizing contribution of the horizontal tail is probably a result of the fact that the tail is moving away from the vortex core more rapidly than the vortex strength is increasing.

Effect of Tail Length

Since the vortex cores, after leaving the trailing edge of the wing, move downstream in approximately a streamwise direction, an increase in

tail length will proportionally increase the vertical distance from the
vortex center to the tail at any given angle of attack. This movement
of the tail relative to the vortex core would be expected to produce a
corresponding increase in tail effectiveness.

A comparison of the data in figures 9(a) and 9(b) shows that for
the two higher tail locations, large decreases in downwash angles occur
as the survey plane is moved from $0.5\bar{c}$ to $1.0\bar{c}$ behind the wing. The
value of $d\epsilon_e/d\alpha$, the factor which is significant in the determination
of stability, also decreases, except in the angle-of-attack range from
8° to 16° where the values of $d\epsilon_e/d\alpha$ are nearly the same for the two
survey planes. For both of these tail heights, the values of $d\epsilon_e/d\alpha$ are
sufficiently large at some angles of attack, even for the rear survey
station, that the stability contribution of horizontal tails at these
locations would be poor. For the low tail position, as the survey sta-
tion is moved from $0.5\bar{c}$ to $1.0\bar{c}$, little change occurs either in the
magnitudes of the downwash angles or in the values of $d\epsilon_e/d\alpha$ and the
small changes which do occur are opposite to those anticipated. Also,
the values of $\left(q_t/q\right)_e$ are from 5 to 10 percent higher for the rear
tail position. The low tail was effective throughout the angle-of-attack
range and exhibited about the same tail effectiveness factor as the corre-
sponding tail height in the forward position.

These results show that, of the hypothetical tail configurations
investigated, the low positions would be most desirable. Other data have
shown that flap deflection and proximity to the ground can also have
large effects on the choice of tail location for any given configuration.
No data were obtained in the present investigation to show these effects.

Comparison with Previous Data

Data are available from several other sources on the downwash behind
somewhat similar delta-wing configurations. No previous tests, however,
have been made for a configuration which is the same as that used in the
present investigation, but differences exist in fuselage configuration,
airfoil section, or test conditions. Data are presented in figure 16
from the present investigation and from references 6 and 7, for which the
data are available in the form of effective downwash angles at various
longitudinal distances behind the wing. The data from reference 6 were
obtained in the Langley full-scale tunnel on a 60° delta wing alone having
10-percent-thick circular-arc sections at a Reynolds number of 6×10^6.
The data from reference 7 were obtained in the Langley stability tunnel
on a 60° delta-wing—fuselage configuration having NACA $65_{(06)}$-006.5 air-
foil sections at a Reynolds number of 2×10^6. An examination of the
lift data presented in figure 10 shows appreciable differences between
the data of the present investigation and those from references 6 and 7.

It is not possible to isolate the cause of the differences shown in these data because of the number of differences in configuration and test condition. Effective downwash data from these three sources for a horizontal tail located 0.2 b/2 above the chord plane at constant values of lift coefficient are shown in figure 16. These data show that, in spite of the large differences in lift curves, rather good agreement is obtained in the effective downwash data at a given lift coefficient. Because of the fact that the leading-edge separation vortex dominates the flow for wings of this type (triangular wing having small leading-edge radii), it can be concluded from this agreement that the vortex configuration on these three wings is approximately the same at a given lift coefficient in spite of the large differences in angle of attack at which these lift coefficients occur.

Effects of Tail Area, Aspect Ratio, and Taper Ratio

In order to show qualitatively the effects of changes in tail area, aspect ratio, and taper ratio on the tail effectiveness factor, the spanwise variations of local values of q_t/q and $\epsilon q_t/q$ are shown in figure 10. The previously mentioned effects of changes in tail height are readily apparent from the downwash data shown in this figure. At the high tail location, near the core of the trailing vortex, the downwash is high at the center line, decreases as the distance from the plane of symmetry is increased, and becomes upwash farther outboard. As the tail location is lowered, the spanwise variation is similar, but much more gradual because of the greater distance from the high velocities near the core of the vortex. The increase in intensity and inboard movement of the vortex as the angle of attack is increased are also apparent in these data. Rather large dynamic-pressure defects occur near the vortex core for the high tail location. At the mid and low tail locations no large decreases in dynamic pressure are apparent and the value of q increases as the distance from the plane of symmetry is increased.

In the determination of effective downwash angles and dynamic pressures for a triangular-plan-form tail, an increase in either area or aspect ratio is equivalent to an increase in span. It is obvious from the data shown in figure 10, therefore, that increases in span or in aspect ratio will result in decreases in effective downwash and increases in dynamic pressure for all but the high tail location. Both of these changes will result in an increase in tail effectiveness factor. For the high tail location, increases in tail span to approximately 0.7b at an angle of attack of 8.6° and to approximately 0.4b for 17.2° cause an increase in $d\epsilon_e/d\alpha$ with only small changes in dynamic pressure. If the span is increased beyond these values, the values of both $d\epsilon_e/d\alpha$ and the dynamic pressure decrease sharply. The effect of these abrupt and conflicting changes on the tail effectiveness factor could be evaluated

only by a quantitative analysis of the data. It is expected, however, that the tail effectiveness factor would be small or negative for all reasonable tail spans. Since an increase in taper ratio shifts a greater percentage of the tail area outboard into a region of lower downwash angles, it will also result in an increase in tail effectiveness factor for the two lower tail locations.

The foregoing discussion should provide a reliable qualitative indication of changes in values of q_t and $d\epsilon_e/d\alpha$. However, the section maximum lift coefficient of the tail is not considered. With the large spanwise variations in downwash angles shown in figure 10, it is probable that portions of the tail would be stalled even at relatively low values of effective tail angle of attack.

Canard-Tail, Wing, and Fuselage Combination in Sideslip

Contour charts of downwash, sidewash and dynamic-pressure ratio are presented in figures 11 and 12 for several sideslip angles. The dashed portions of the contours are taken from extrapolated curves and are believed to be representative of the flow in that region. In general, the contours for the model at angles of sideslip of -3.5° and -7.0° are similar to the contours for the 0° sideslip condition. (See figs. 11 and 12.) An examination of the sidewash contours shows that for a given height above the chord plane extended the sidewash angles above the left and right wing tips are approximately equal when referred to the free-stream direction. Even though this is less true for the contours at $\alpha = 25.7°$ than for the contours at $\alpha = 8.6°$, it is an indication that yaw angles of the magnitude tested have very little effect on the forma-tion of the wing separation vortex. Certain detail changes occur in the flow field as the yaw angle changes which can be attributed to this tend-ency of the flow to follow the stream direction and to remain constant in planes perpendicular to the flow. These changes are most apparent near the fuselage where the cross flow is a direct function of sideslip angle.

The effect of the canard tail is apparent in the flow above the wing at an angle of attack of 8.6°. A region of reduced dynamic pressure is observed in the flow above the wing-chord plane at the plane of symmetry and moves to the right and up as the sideslip angle is increased. Since this wake from the canard tail moves downstream in approximately the stream direction, an increase in angle of attack to 25.7° places it in a position above the region surveyed.

In order to examine further the effects of the flow phenomena involved, plots of sidewash angle against vertical height have been made for sideslip angles of -3.5° and -7.0° at $\alpha = 8.6°$ and 25.7°, respec-tively. At each combination of angles, plots were made for a vertical

tail located on the plane of symmetry and for a set of outboard fins at 55 percent of the semispan. The sidewash angles presented are referred to the axis of symmetry of the model and therefore represent local angles of attack for a vertical fin.

For the central tail position at $\alpha = 8.6^\circ$, figure 13(a) shows that the effective angle of attack of the vertical tail increases in proportion to the sideslip angle and that the local angle remains relatively constant along the tail span. As the angle of attack is increased to $\alpha = 25.7^\circ$, the wing separation vortex grows to cover larger portions of the flow above the wing so that the effect of yawing the model is to cause the influence of the vortex to be felt more strongly at the central tail position. An examination of figure 13(b) shows that this flow is characterized by large values and steep gradients in sidewash angle with a reversal of flow occurring for the central portions of the region surveyed. However, unlike the flow for $\alpha = 8.6^\circ$, an increase in sideslip angle from -3.5° to -7.0° does not produce a proportional change in the average value of sidewash angle.

As seen from the contours, the outboard fins, by virtue of their proximity to the wing vortex center, are located in a more unfavorable flow field than a centrally located vertical tail. The contours also indicate an increase in dissimilarity of the flow above the left and right wing with increase in angle of attack. For a specific study of the flow for the 0.55b/2 station, figure 13 shows that for $\alpha = 8.6^\circ$, the left fin position, due to higher average sidewash angle, is more effective than the central tail location and that the effective angle of attack increases with increase in sideslip angle. The right fin position shows little or no effectiveness at -3.5° sideslip but approximately the same change in effective angle of attack as the sideslip angle changes from -3.5° to -7°. At an angle of attack of 25.7°, the spanwise variation of sidewash angles is indicative of a strong vortex flow. The vortex configuration is such that the effective angles of attack of the right and left fins are opposed to each other and the total contribution to yawing moment is reduced to a very small value. A change in sideslip angle in the range tested has little effect on these flow characteristics. It should be realized that these surveys show the effect of the model at an angle of sideslip without vertical tails in place and that the addition of vertical fins, (the outboard fins more than a centrally located tail) may alter the flow field. It is also interesting to note the large vertical extent of the spanwise flow which occurs above the wing at an angle of attack of 25.7°.

Effect of Canard Tail on Effective Angle of Attack of the Wing

In order to show the effect of a canard tail surface on the flow characteristics at the wing, downwash angles were measured in a plane $1.93\bar{c}$

behind the nose of the body—canard-tail combination (fig. 3) at several angles of attack. These data are presented as contours of downwash angle ϵ' in figure 14. An examination of the data in figure 14 shows that a wing located in a high, mid, or low position on the fuselage would experience approximately the same flow angles. The region of highest downwash occurs at about $0.25b/2$ above the chord plane for an angle of attack of 8° and moves higher as the angle of attack is increased. Values of ϵ (referred to the free-airstream direction) for the midwing location are shown in figure 15. These data show that the wing experiences an upwash over the greater part of its span for all the angles of attack tested. The angularity of the flow produced by the fuselage alone was computed by the approximate method presented in reference 8 and is also shown in figure 15. The method of reference 8 assumes the flow at any axial location to be the same as the flow about an infinite cylinder having the same diameter as the local body diameter. If the computed values are assumed to give a reliable indication of the flow about the body, the difference between the computed and the experimental curves for any particular angle of attack represents the change in the flow field produced by the canard tail. This difference shows a downwash at inboard stations which decreases for positions farther outboard and becomes upwash, for most of the angles of attack considered, at positions outboard of the center of the trailing vortex from the canard tail. The flow angles which can be attributed to the effect of the canard tail are rather small and should cause no great change in wing characteristics for the conditions tested. For conditions where the canard tail is deflected at low angles of attack, however, the large flow angles existing near the core of the trailing vortex could have a more pronounced effect on the wing characteristics.

CONCLUSIONS

An investigation at low speeds and a Reynolds number of 9×10^6 of the flow field behind the lifting surfaces of a model equipped with a 60° triangular wing and a 60° triangular canard tail has produced the following conclusions:

1. Effective downwash angles obtained from tests of 60° triangular wings experiencing the separation-vortex type of flow but having various combinations of fuselage, airfoil section, or test conditions seem to agree with each other at given values of lift coefficient, regardless of rather large differences in the angle of attack at which these lift coefficients occur.

2. For an unflapped triangular wing away from the influence of the ground, horizontal tails located at 0.5 mean aerodynamic chord and 1.0 mean aerodynamic chord behind the wing trailing edge should be

placed below the wing-chord plane, as shown by previous investigations at low Reynolds number.

3. Analysis of the survey data shows generally that increases in the area, aspect ratio, or taper ratio of a rear horizontal tail produce an increase in the tail effectiveness factor $\left(1 - \dfrac{d\epsilon_e}{d\alpha}\right)(q_t/q)_e$.

4. At high angles of attack, the inboard movement of the main wing separation vortex is such as to cause large interference with vertical tails mounted either centrally or outboard on the wing.

5. The flow field from the canard tail at $0°$ deflection has little effect on the flow over the wing.

Langley Aeronautical Laboratory,
    National Advisory Committee for Aeronautics,
        Langley Field, Va.

REFERENCES

1. Bird, John D., and Riley, Donald R.: Some Experiments on Visualization of Flow Fields Behind Low-Aspect-Ratio Wings by Means of a Tuft Grid. NACA TN 2674, 1952.

2. Glauert, H.: Wind Tunnel Interference on Wings, Bodies and Airscrews. R. & M. No. 1566, British A.R.C., 1933.

3. Herriot, John G.: Blockage Corrections for Three-Dimensional-Flow Closed-Throat Wind Tunnels, With Consideration of the Effect of Compressibility. NACA Rep. 995, 1950. (Supersedes NACA RM A7B28.)

4. Katzoff, S., and Hannah, Margery E.: Calculation of Tunnel-Induced Upwash Velocities for Swept and Yawed Wings. NACA TN 1748, 1948.

5. Spreiter, John R., and Sacks, Alvin H.: The Rolling Up of the Trailing Vortex Sheet and Its Effect on the Downwash Behind Wings. Jour. Aero. Sci., vol. 18, no. 1, Jan. 1951, pp. 21-32, 72.

6. Whittle, Edward F., Jr., and Hawes, John G.: Investigation at Low Speed of the Downwash, Sidewash, and Wake Characteristics Behind a Large-Scale Triangular Wing, Including the Effects of Yaw, Full-Span Trailing-Edge Flaps, and Two Leading-Edge Modifications. NACA RM L52H19, 1952.

7. Jaquet, Byron M.: Effects of Horizontal-Tail Position, Area, and Aspect Ratio on Low-Speed Static Longitudinal Stability and Control Characteristics of a 60° Triangular-Wing Model Having Various Triangular-All-Movable Horizontal Tails. NACA RM L51I06, 1951.

8. Hopkins, Edward J., and Carel, Hubert C.: Experimental and Theoretical Study of the Effects of Body Size on the Aerodynamic Characteristics of an Aspect Ratio 3.0 Wing-Body Combination. NACA RM A51G24, 1951.

TABLE I

DIMENSIONS OF TRIANGULAR-WING MODEL USED FOR FLOW SURVEYS

Wing:
    Area, sq in.(to fuselage center line)   144
    Span, in. 18.24
    Mean aerodynamic chord, in. 10.54
    Aspect ratio 2.31
    Sweepback of leading edge, deg   60
    Taper ratio   0
    Dihedral, deg   0
    NACA airfoil section 65A006

Fuselage:
    Length, in. 33.33
    Maximum diameter, in.   3.33
    Fuselage frontal area/wing plan-form area 0.0606

Canard Horizontal Tail:
    Area, sq in. (to fuselage center line) 28.80
    Span, in. 8.16
    Mean aerodynamic chord, in. 4.71
    Aspect ratio 2.31
    Sweepback of leading edge, deg   60
    Taper ratio   0
    NACA airfoil section 65A006
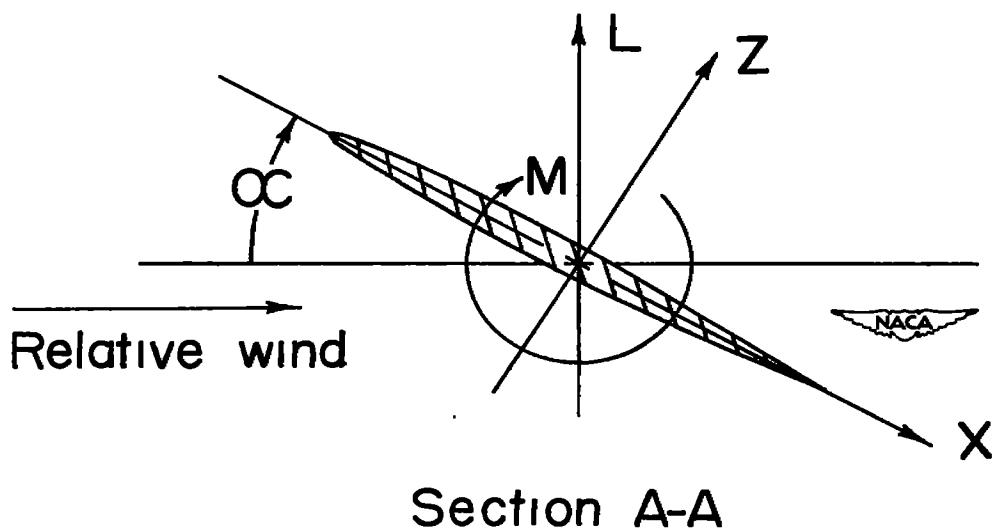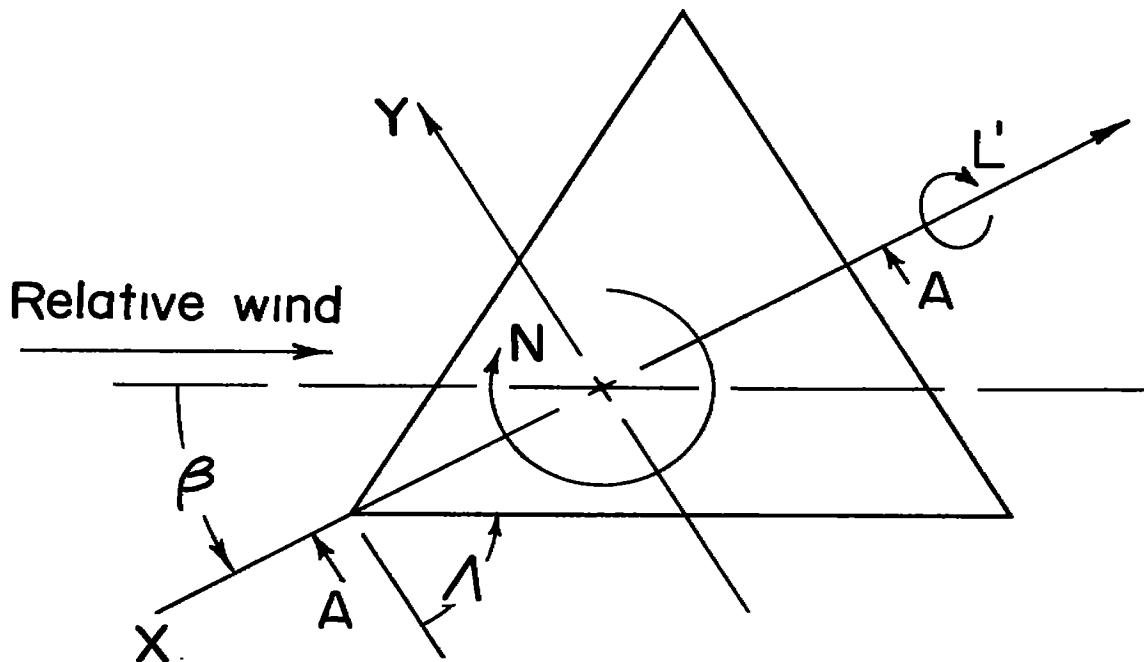
Figure 1.- Body axes. Positive forces, moments, and angles are indicated.
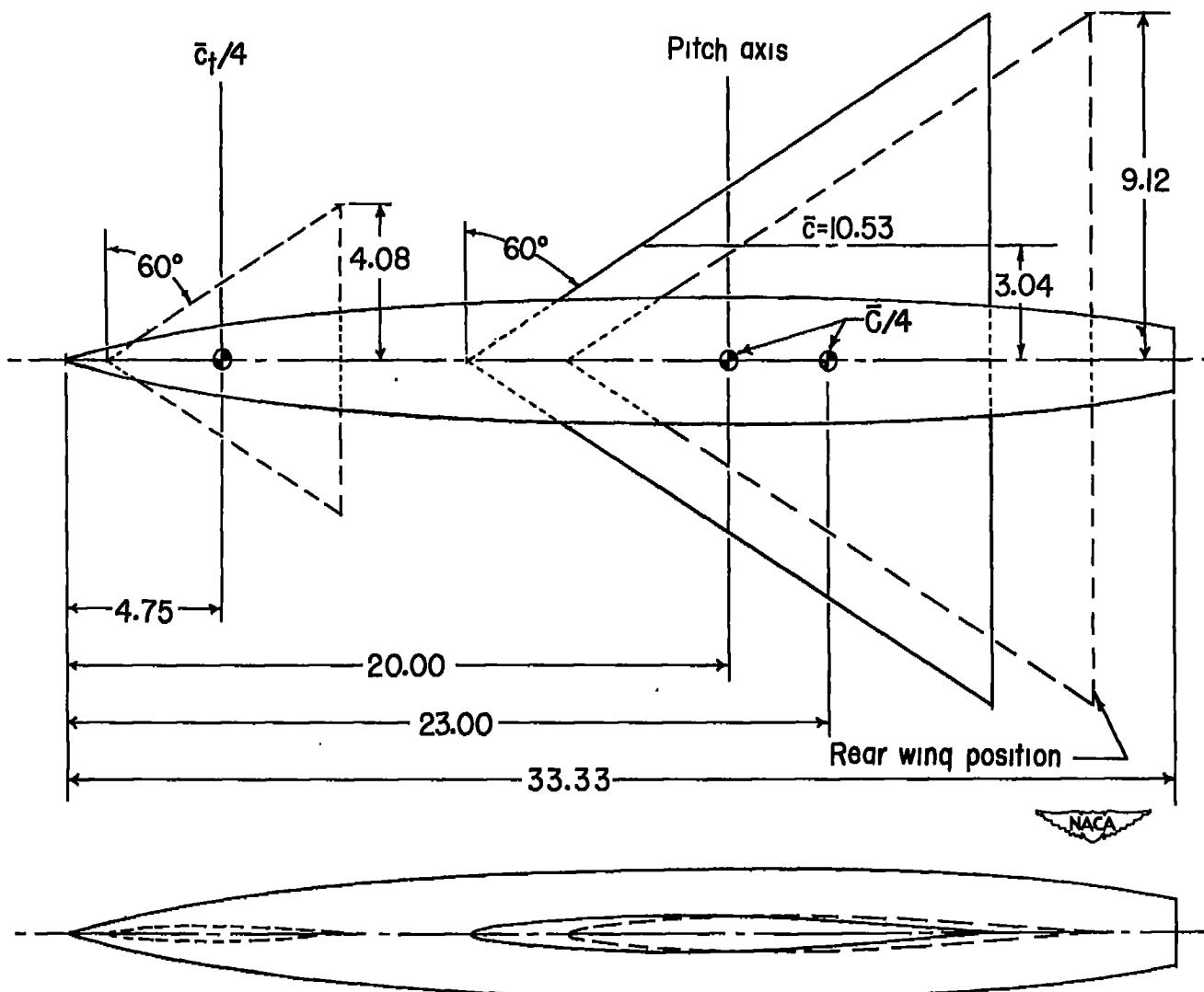
Figure 2.- Sketch of triangular-wing model used for flow surveys.
All dimensions are in inches.
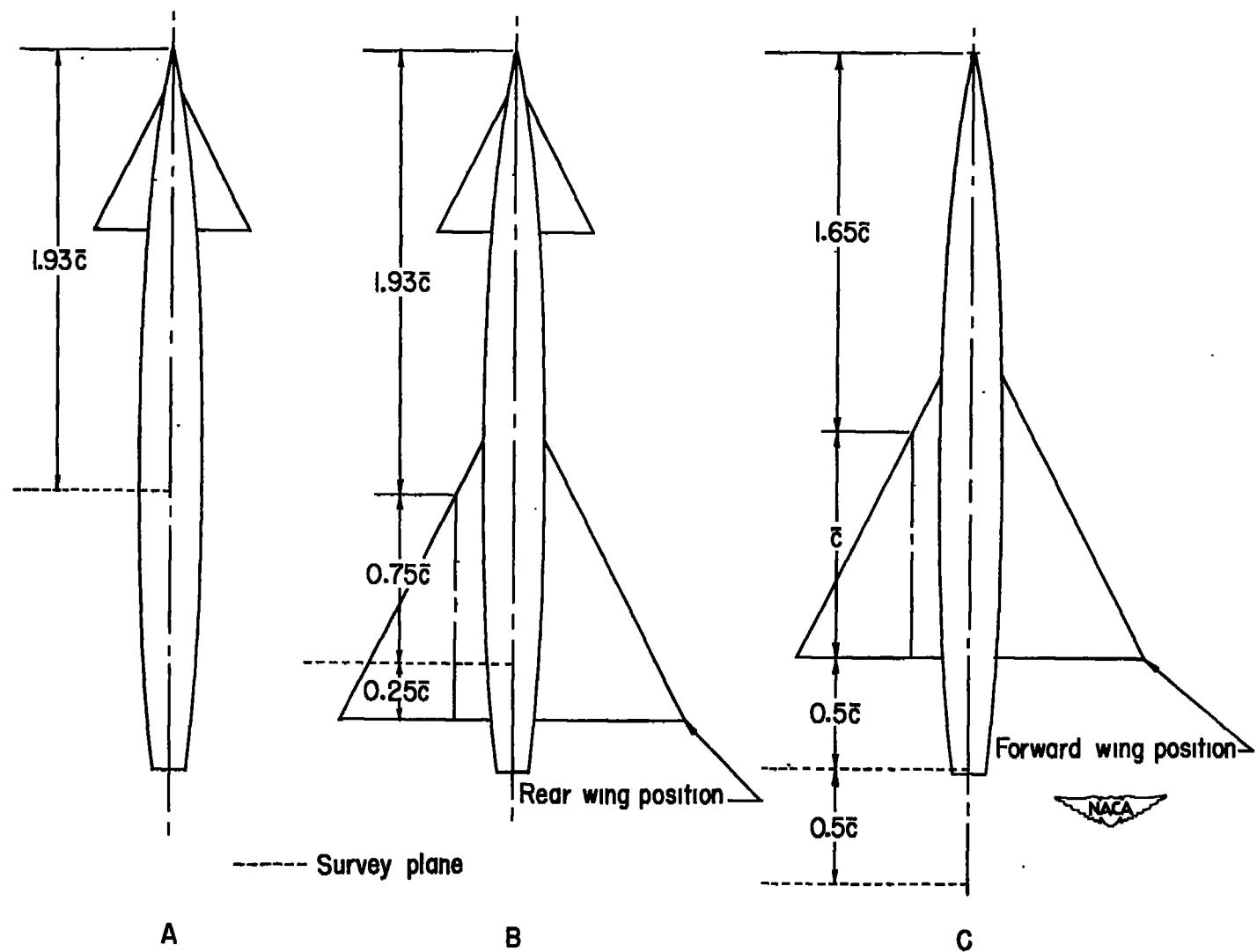
Figure 3.- Location of vertical survey planes for various model configurations.
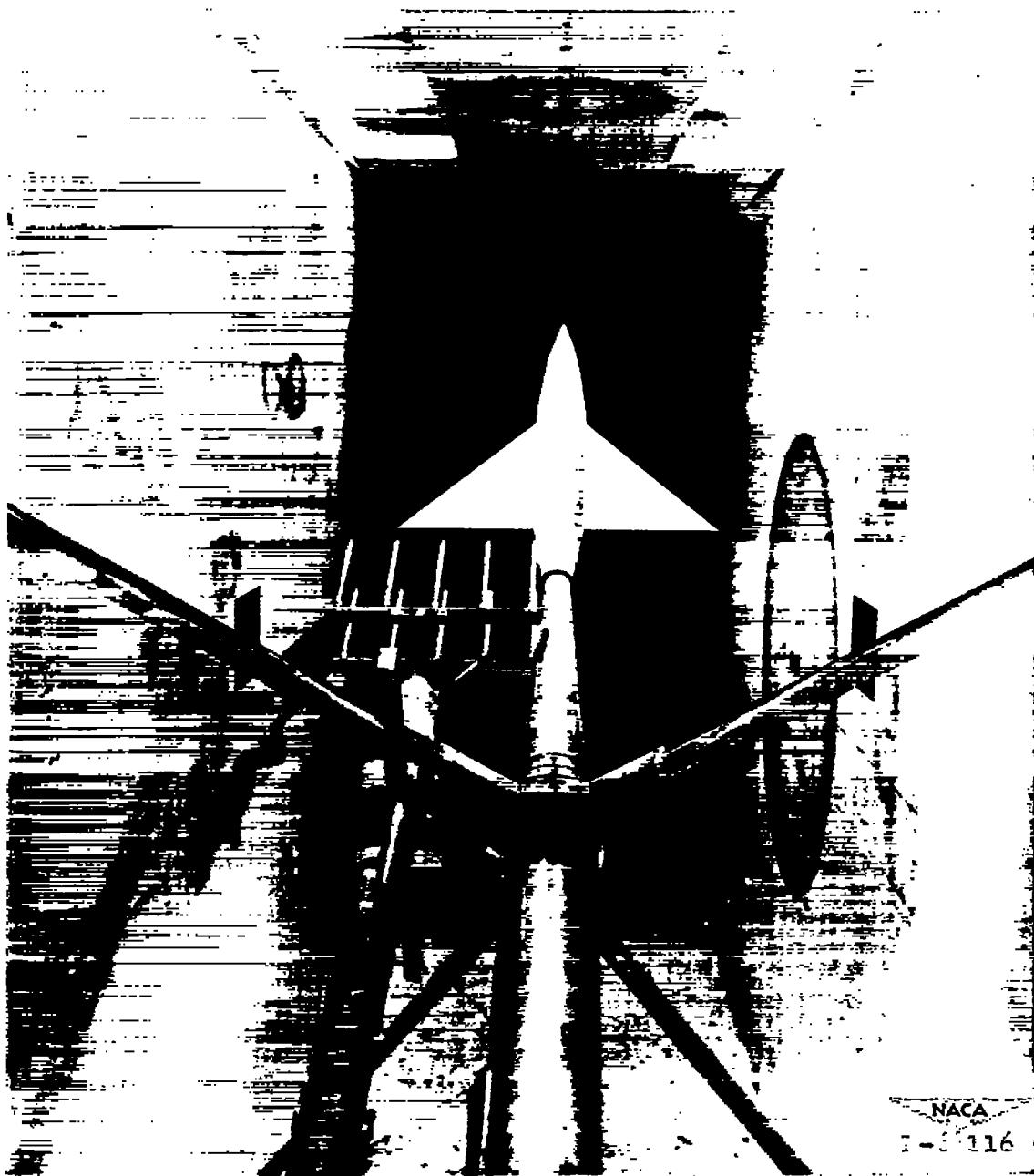
(a) Survey rake mounted behind the 60° triangular wing.

Figure 4.- The 60° triangular-wing model with flow-survey apparatus mounted in the Langley low-turbulence pressure tunnel.
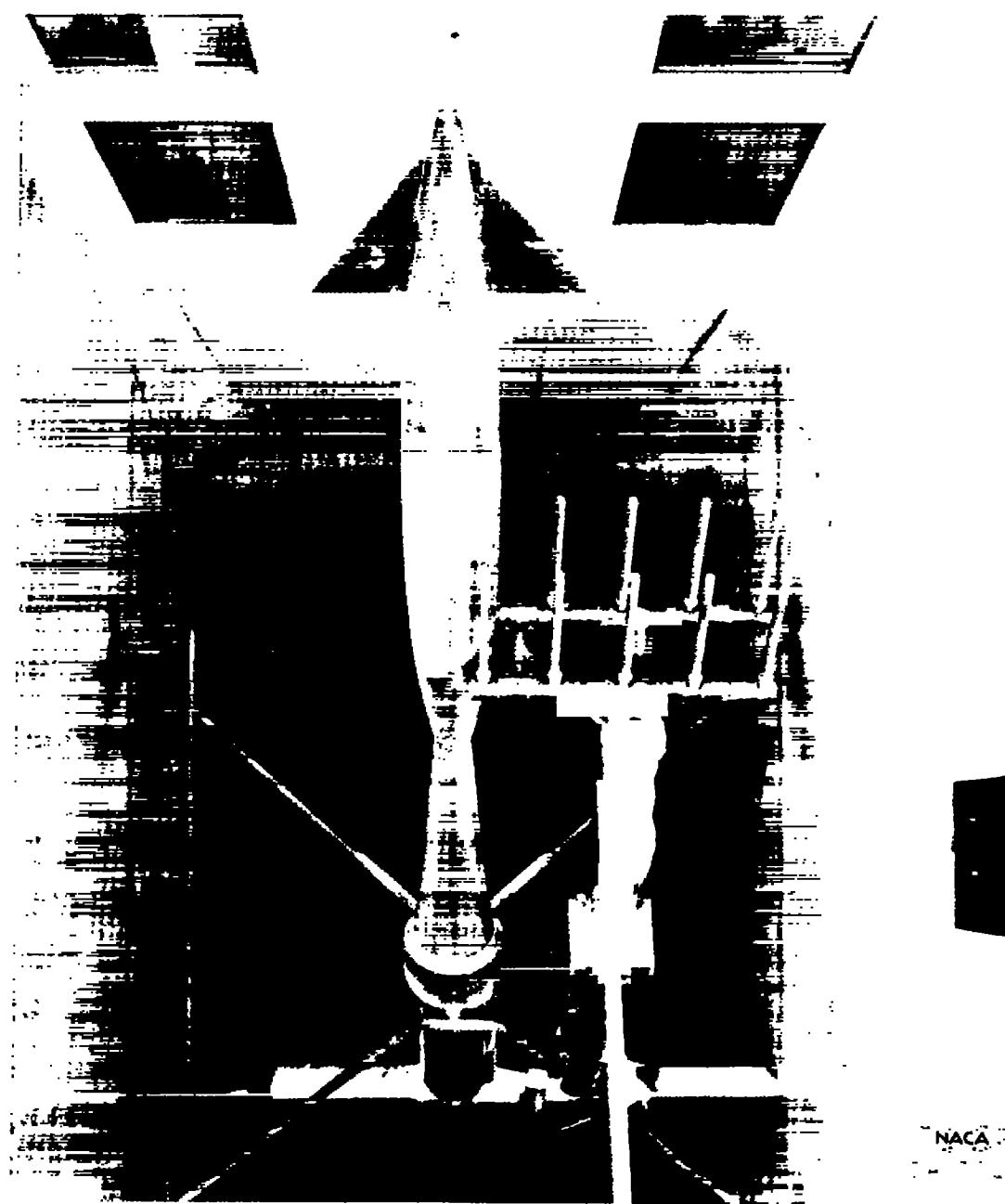
(b) Survey rake mounted behind a 60° triangular wing used as a canard tail.

Figure 4.- Concluded.
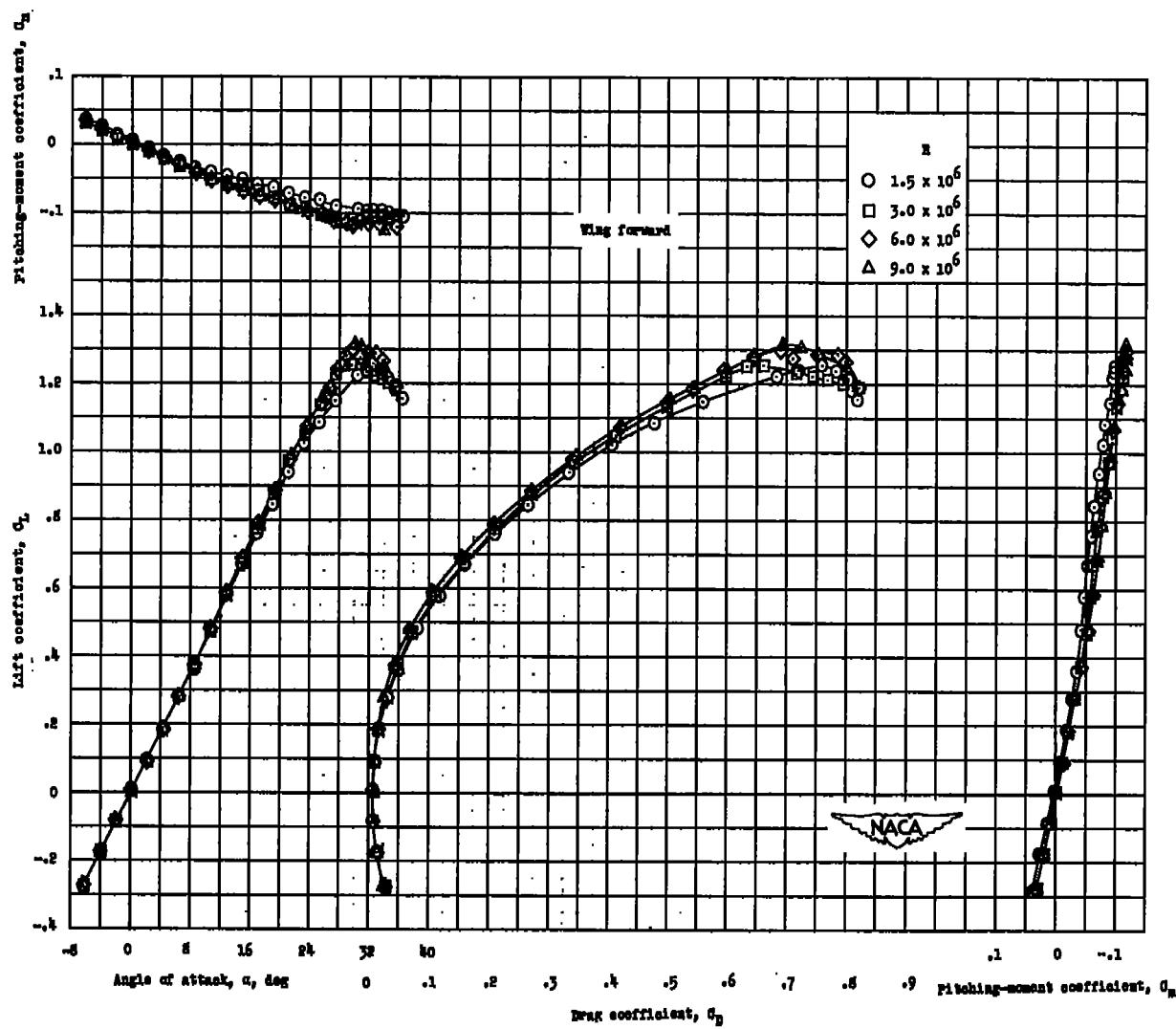
Figure 5.- Effect of Reynolds number on the aerodynamic characteristics of a 60° delta wing-fuselage model.
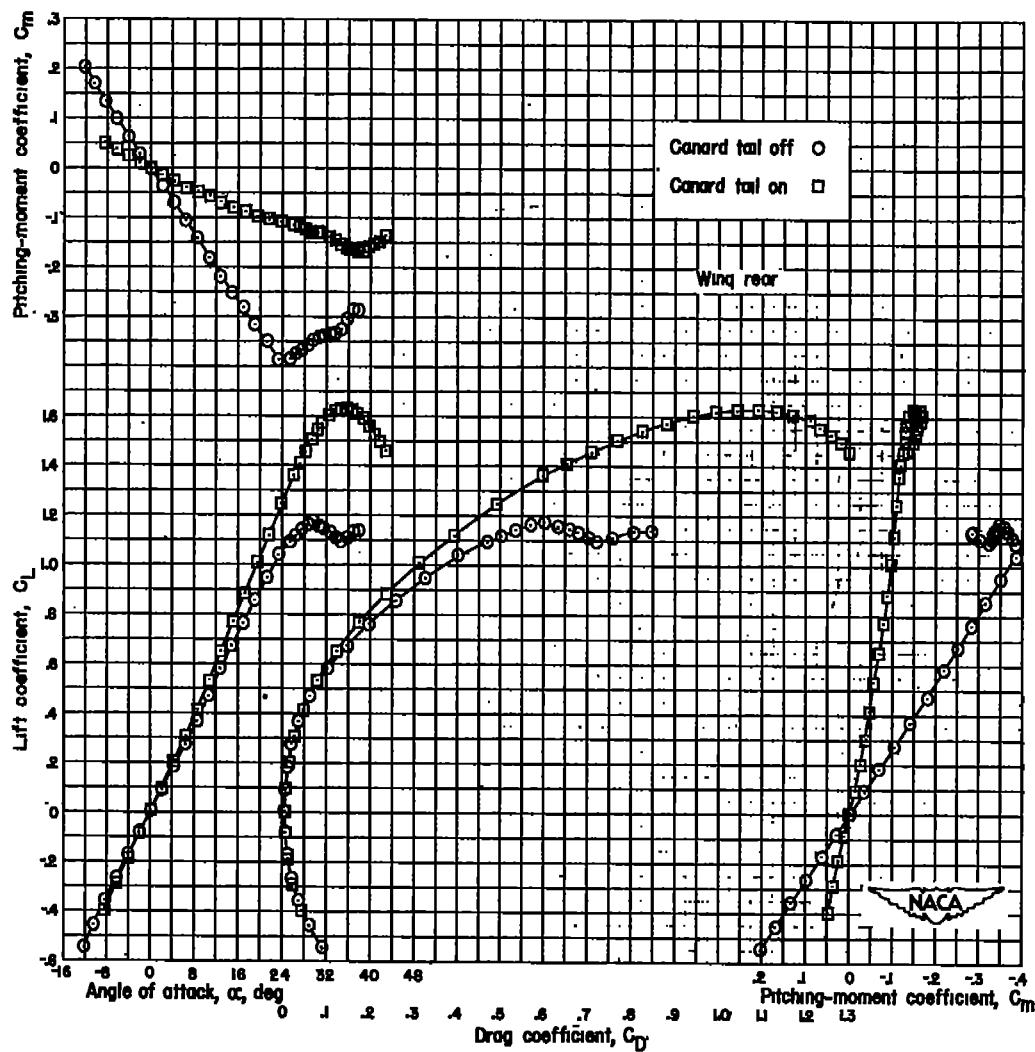
Figure 6.- Effect of a canard tail on the aerodynamic characteristics of a 60° delta-wing model. R = 9.0 × 10⁶.

Vertical distance from chord plane extended, $\frac{z}{b/2}$

Lateral distance from plane of symmetry, $\frac{y}{b/2}$

Vortex core

Angle of downwash, ε', deg

Angle of sidewash, σ', deg

Dynamic-pressure ratio, q_t/q

NACA
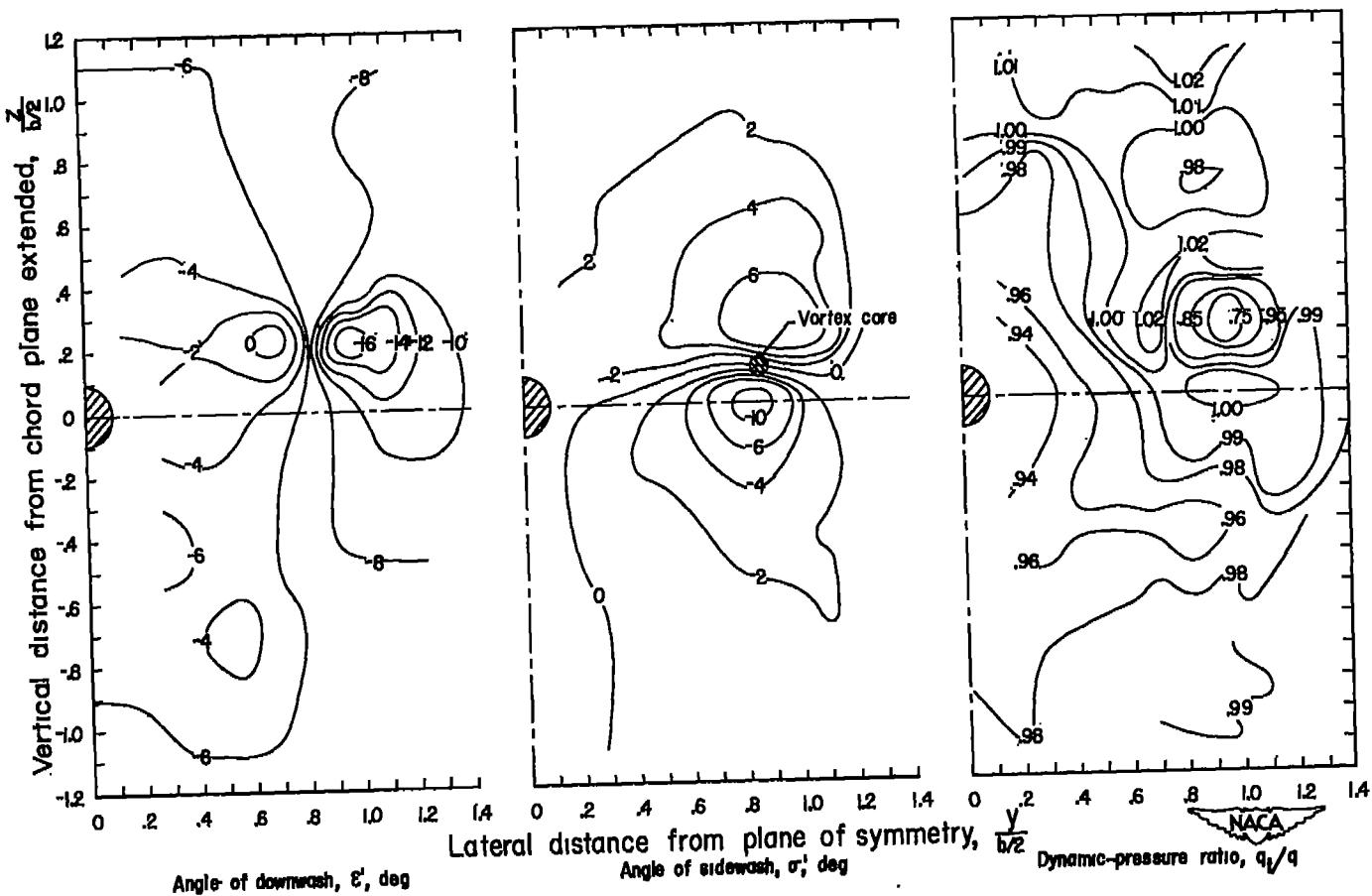
(a) $\alpha = 8.6°$; $C_L = 0.37$.

Figure 7.- Contour charts of downwash angle, sidewash angle, and dynamic-pressure ratio for a $60°$ delta-wing—fuselage model. Plane of survey located at $0.5\bar{c}$ behind wing trailing edge. $\beta = 0°$; $R = 9.0 \times 10^6$; configuration C.

Angle of downwash, ε', deg

Angle of sidewash, σ', deg

Dynamic-pressure ratio, q_t/q

Lateral distance from plane of symmetry, $\dfrac{y}{b/2}$
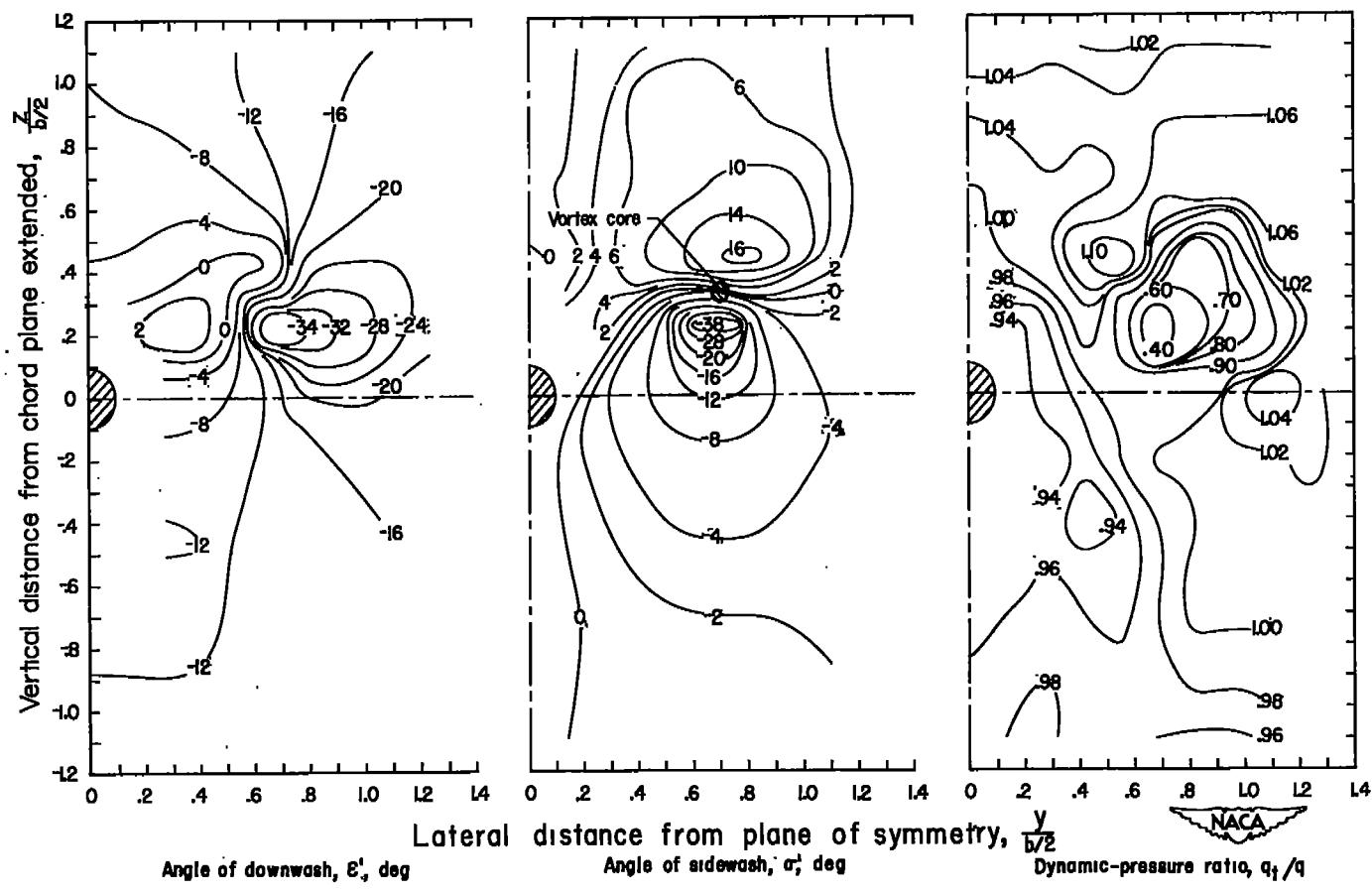
(b) $\alpha = 17.2°$; $C_L = 0.79$.

Figure 7.- Continued.

Lateral distance from plane of symmetry, $\frac{y}{b/2}$

Angle of downwash, ε, deg   Angle of sidewash, σ, deg   Dynamic-pressure ratio, q_t/q
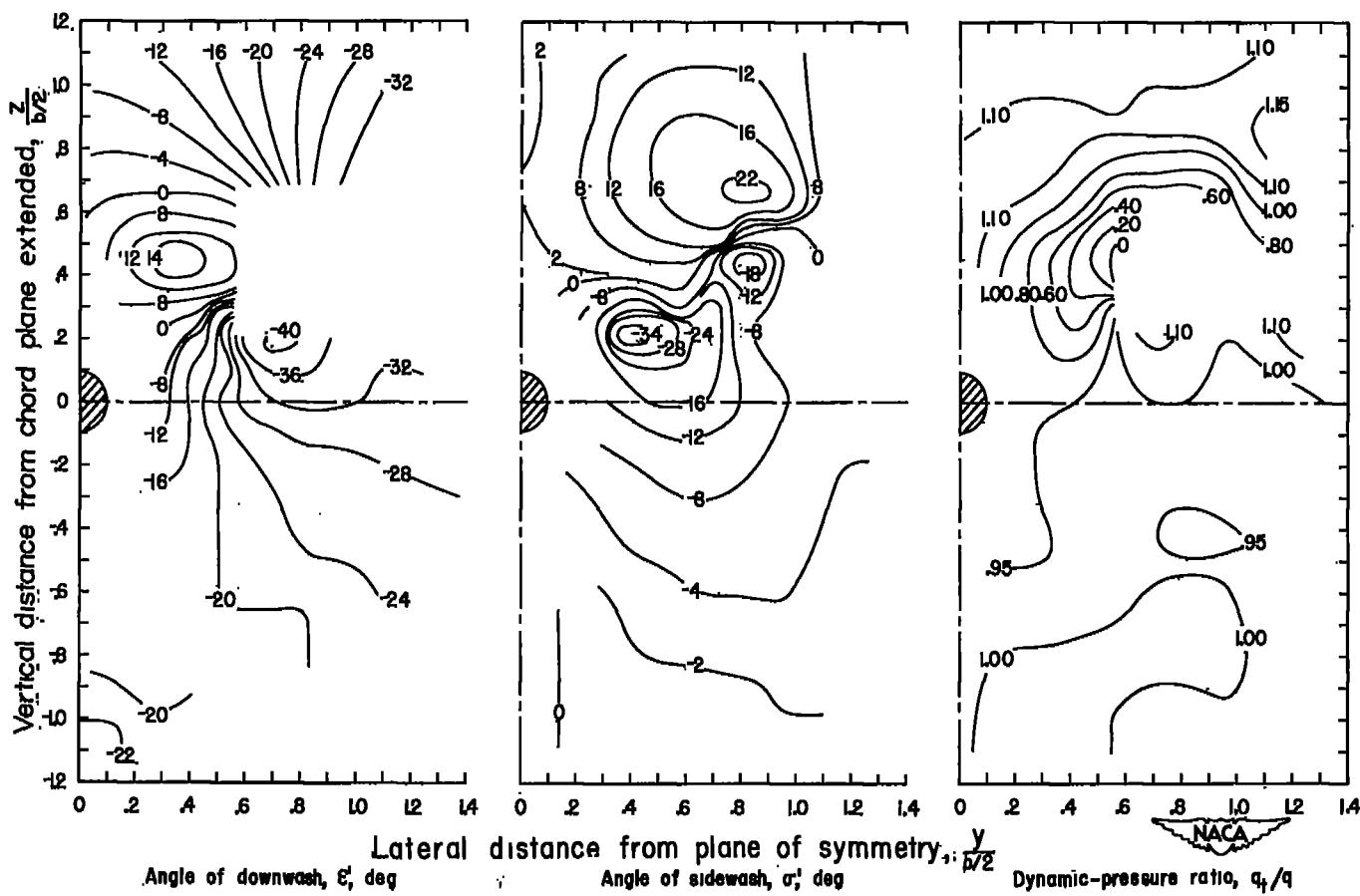
(c) $\alpha = 25.7°$; $C_L = 1.15$.

Figure 7.- Continued.

Angle of downwash, ε', deg   Angle of sidewash, σ', deg   Dynamic-pressure ratio, q_t/q

Lateral distance from plane of symmetry, $\frac{y}{b/2}$
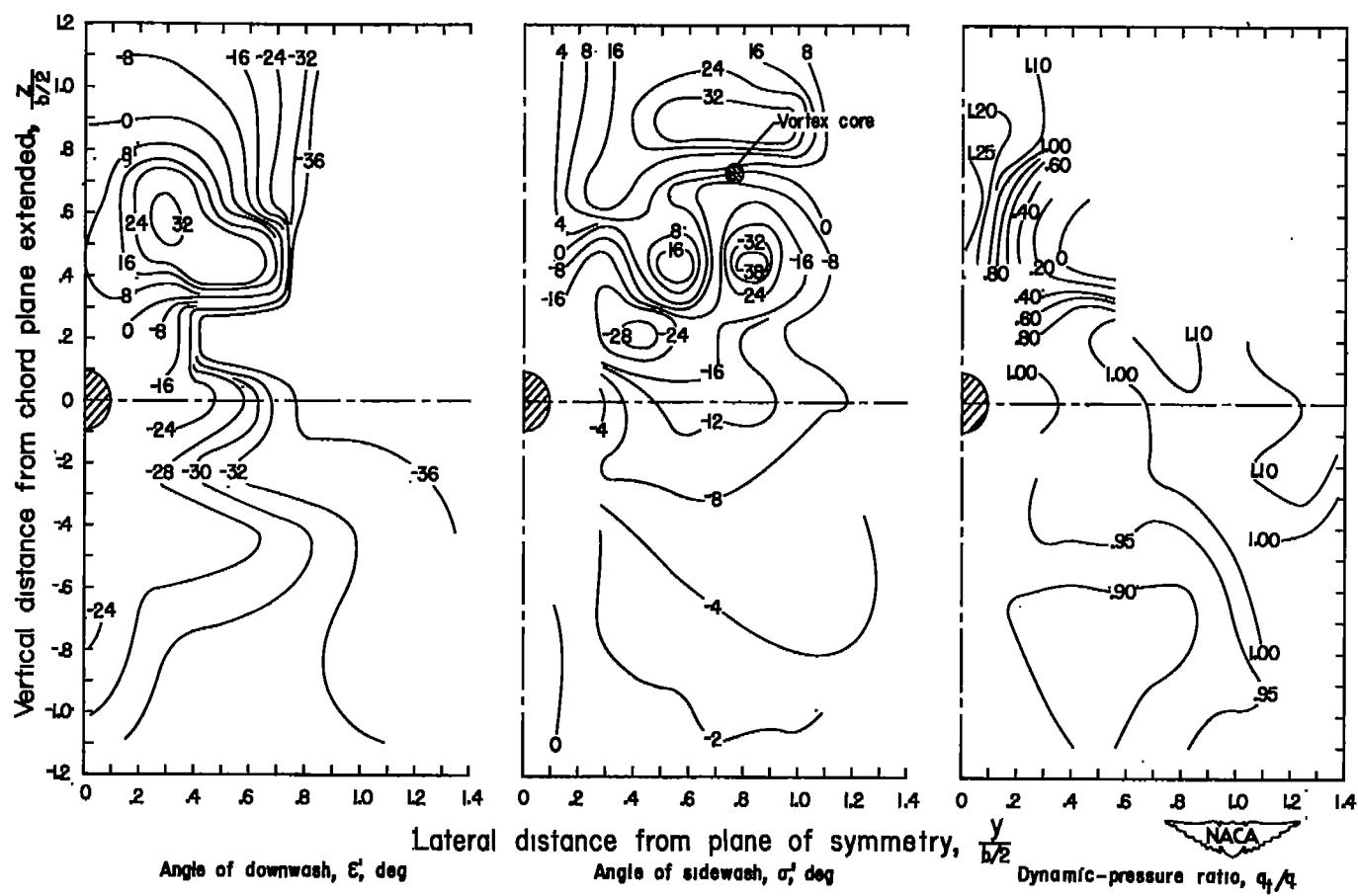
(d) $\alpha = 33.9°$; $C_L = 1.25$.

Figure 7.- Concluded.
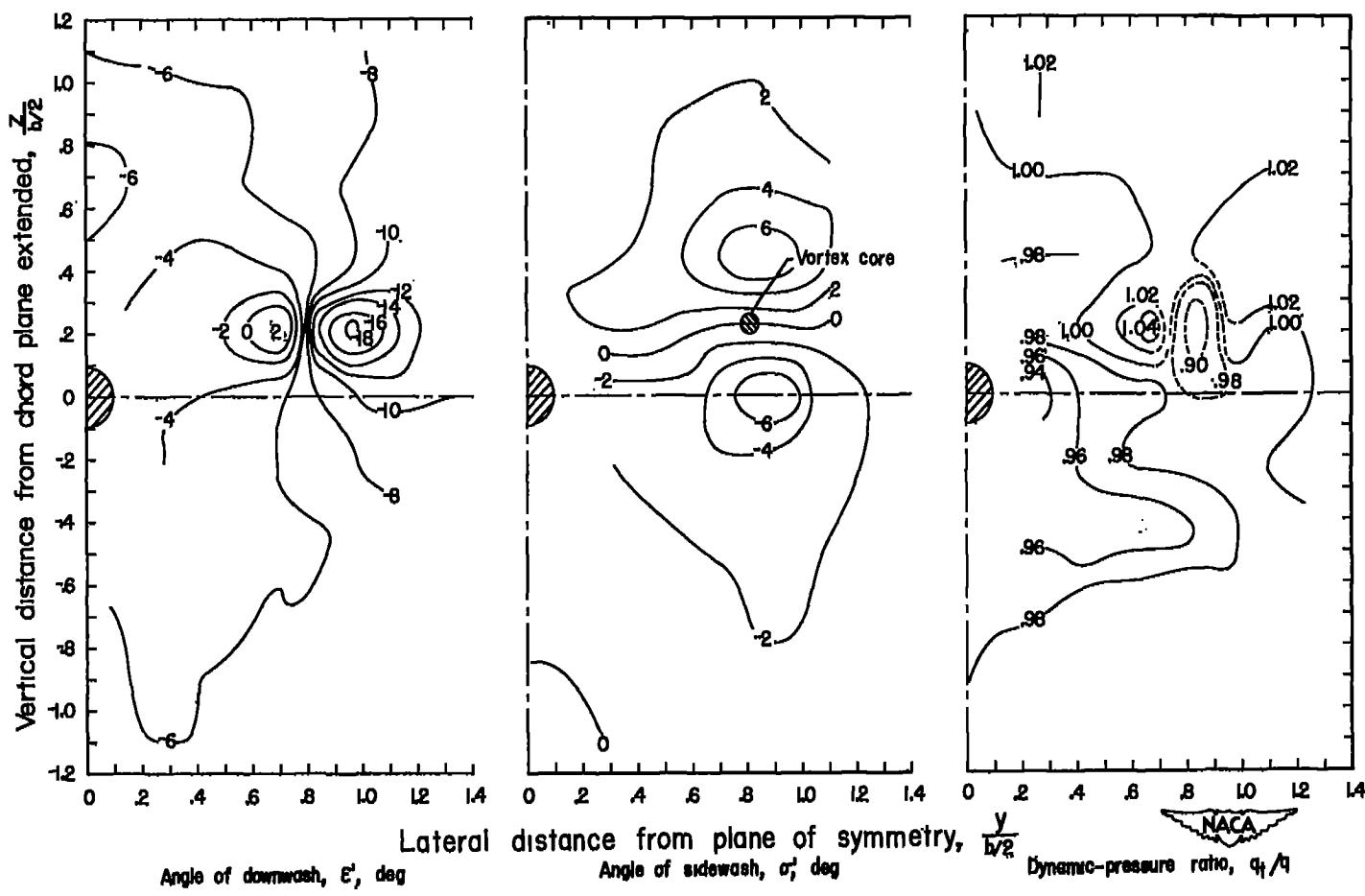
(a) $\alpha = 8.6°$; $C_L = 0.37$.

Figure 8.- Contour charts of downwash angle, sidewash angle, and dynamic-
pressure ratio for a $60°$ delta-wing—fuselage model. Plane of survey
located at $1.0\bar{c}$ behind wing trailing edge. $\beta = 0°$; $R = 9.0 \times 10^6$;
configuration C.

Vertical distance from chord plane extended, $\frac{z}{b/2}$

Angle of downwash, ϵ', deg

-8
-12
-16
-20
-24
-28
-36
-4
0 4
-4
-8
-12
-16
-20
-24

Vortex core

Angle of sidewash, σ', deg

4
4
0
-8
-16
-24
-20
-12
-2
-2
-4
0
0

Dynamic-pressure ratio, q_k/q

1.04
1.06
1.02
1.04
1.00
.96
.92
.96
.88
.94
1.02
1.00
1.08
1.00
1.00
1.06
1.04
.98
.96
.94
.98
1.00
1.00
.98

Lateral distance from plane of symmetry, $\frac{y}{b/2}$

NACA
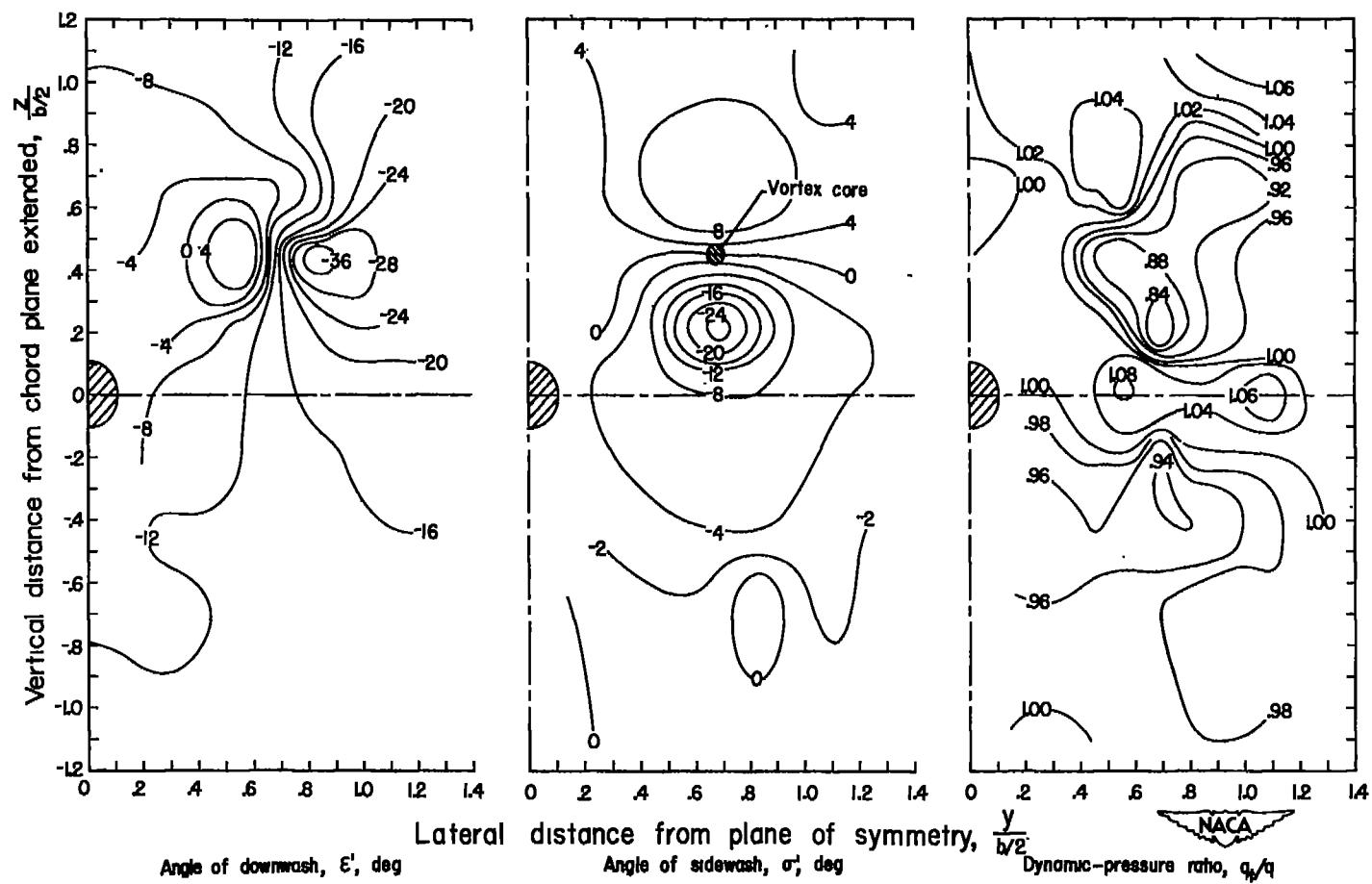
(b) $\alpha = 17.2^\circ$; $C_L = 0.79$.

Figure 8.- Continued.
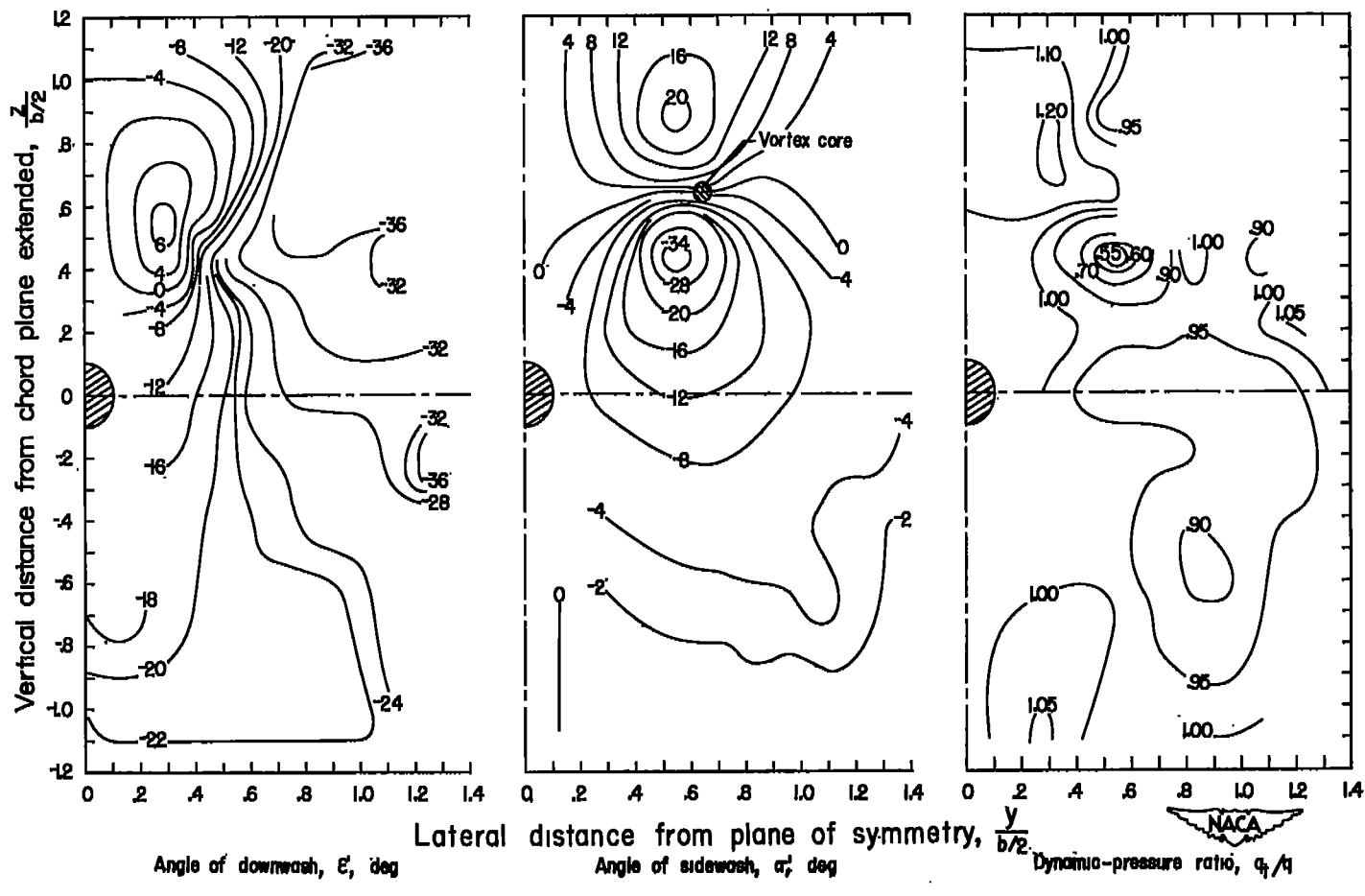
(c) $\alpha = 25.7°$; $C_L = 1.15$.

Figure 8.- Continued.

Lateral distance from plane of symmetry, $\frac{y}{b/2}$

Angle of downwash, ε', deg

Angle of sidewash, σ', deg

Dynamic-pressure ratio, q_t/q
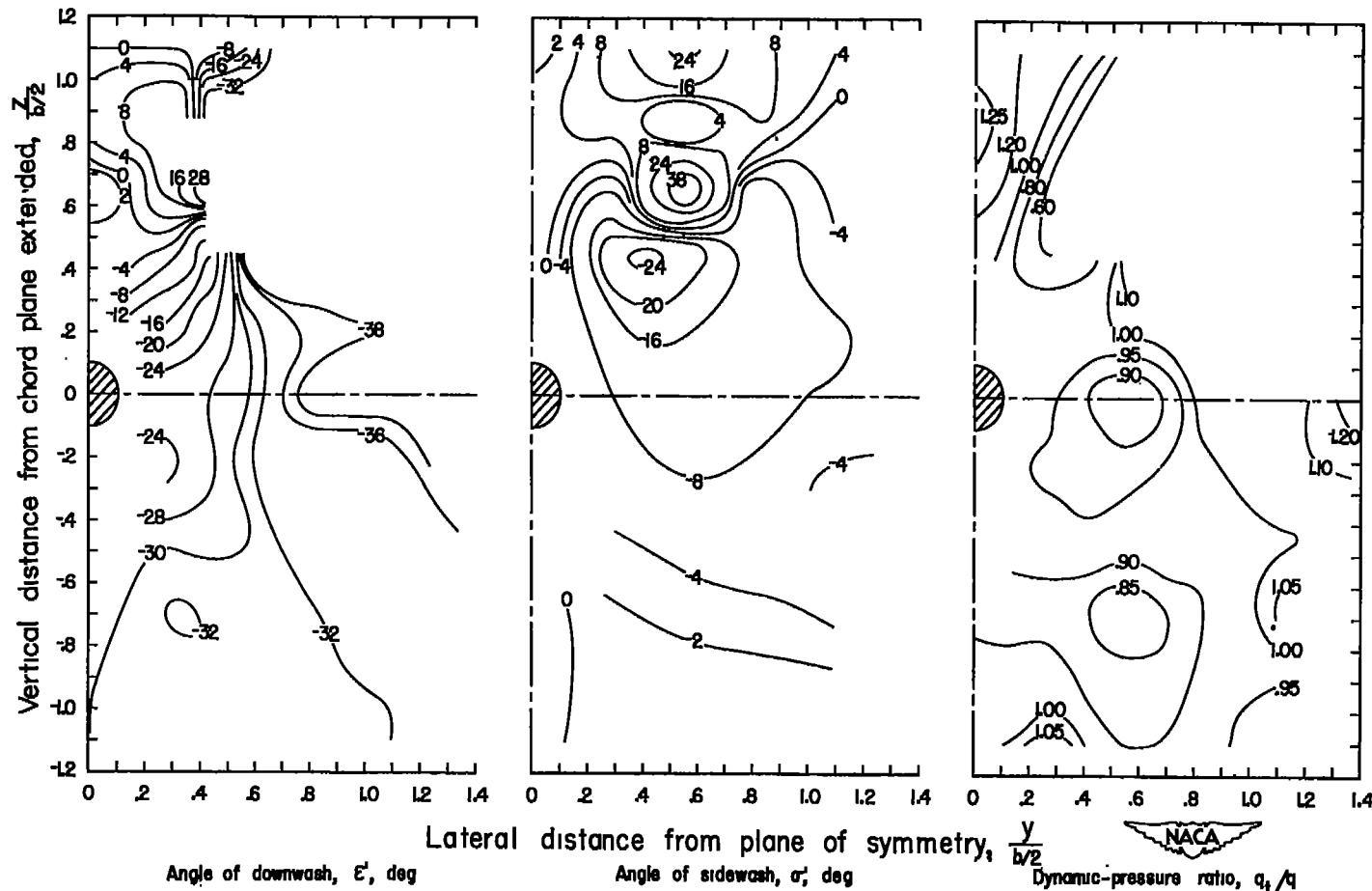
(d) $\alpha = 33.9^\circ$; $C_L = 1.25$.

Figure 8.- Concluded.
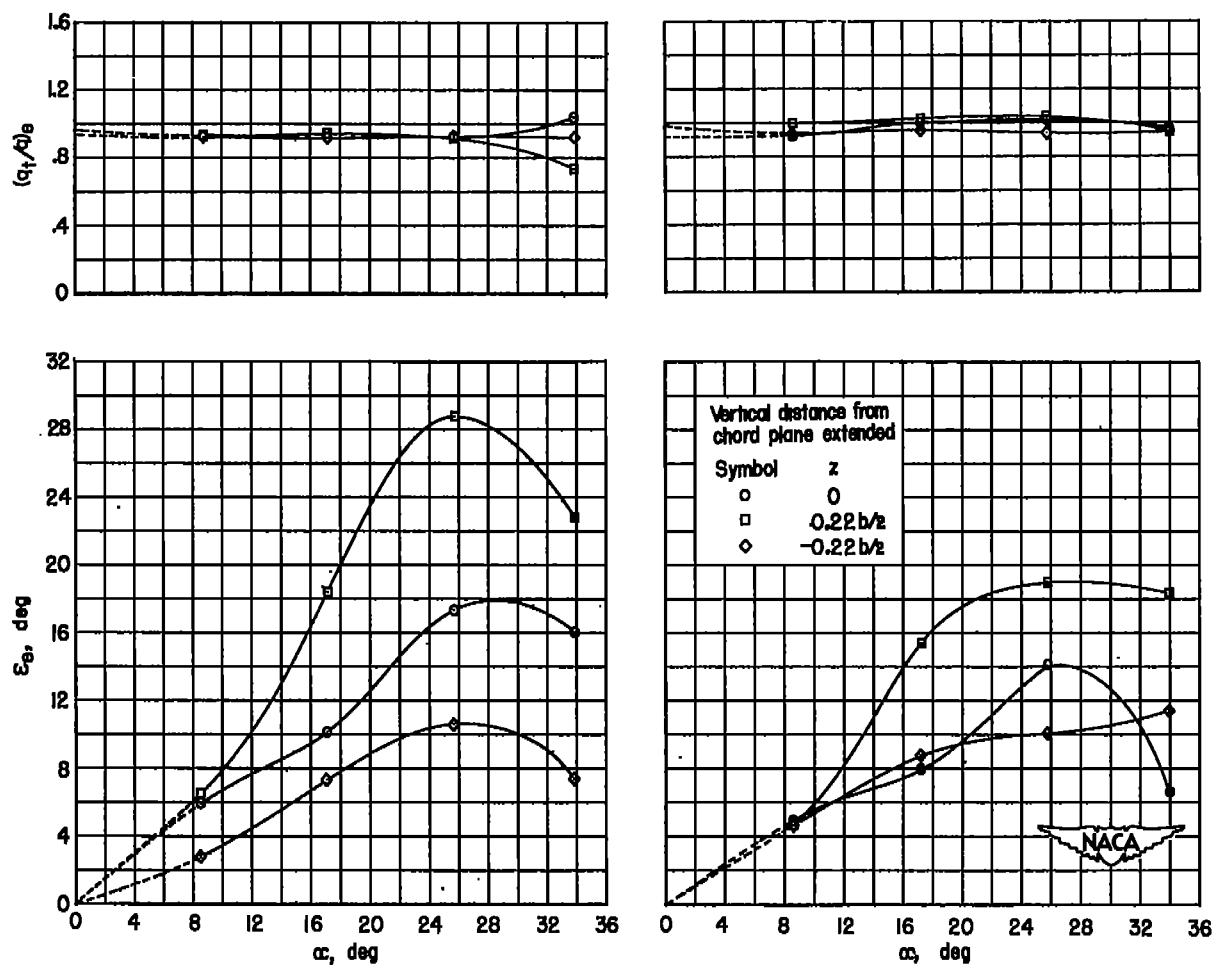
(a) Plane of survey $0.5\bar{c}$ behind wing trailing edge.

(b) Plane of survey $1.0\bar{c}$ behind wing trailing edge.

Figure 9.- Variation of effective downwash angle and dynamic-pressure ratio with angle of attack.
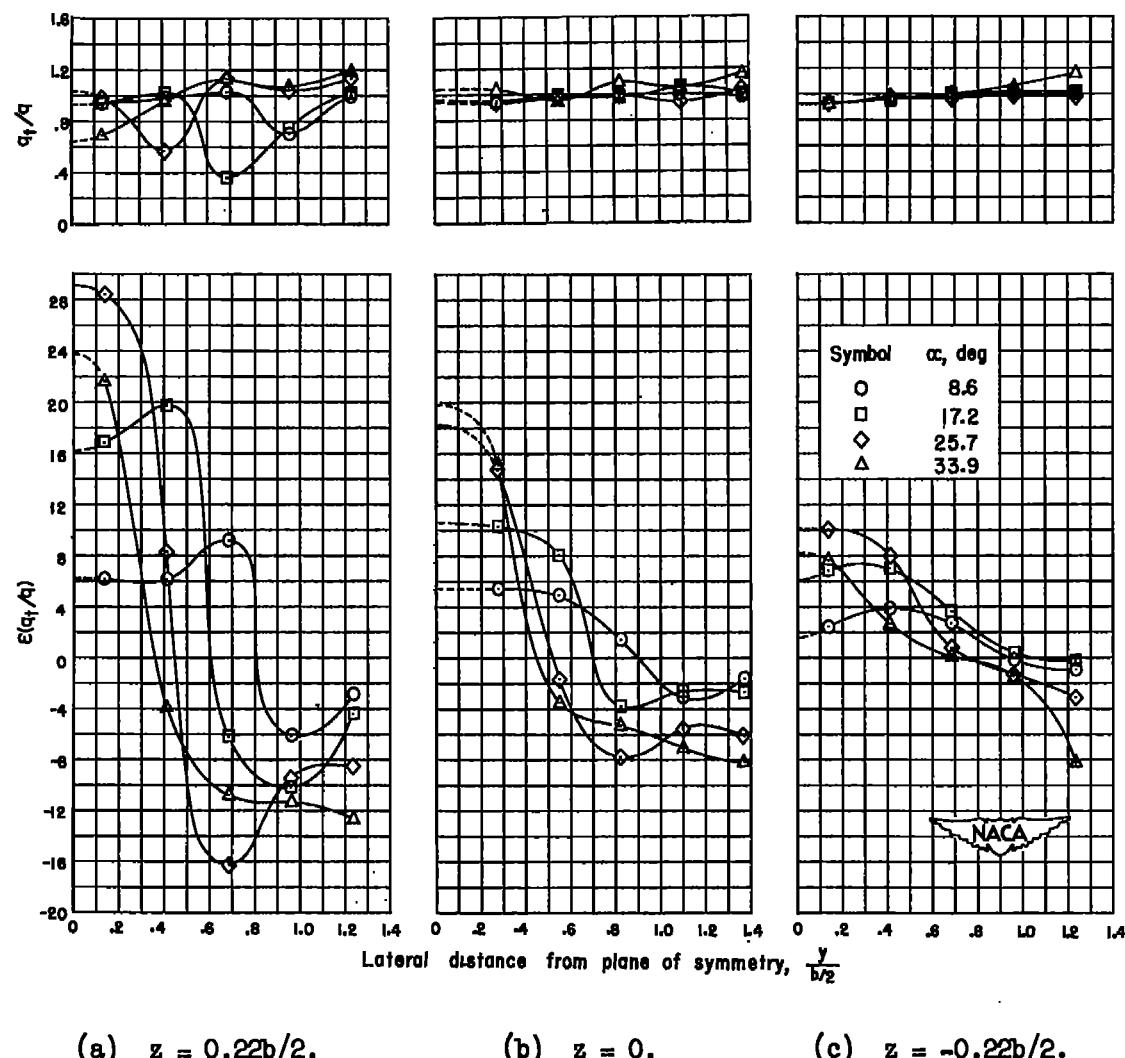
(a) z = 0.22b/2.   (b) z = 0.   (c) z = -0.22b/2.

Figure 10.- Variation of q_t/q and $\epsilon(q_t/q)$ with lateral distance for survey plane located at 0.5c̄ behind wing trailing edge.

Angle of downwash, ϵ', deg

Angle of sidewash, σ', deg

Dynamic-pressure ratio, q_t/q

Lateral distance from plane of symmetry; $\dfrac{y}{b/2}$

Vertical distance from chord plane extended, $\dfrac{z}{b/2}$
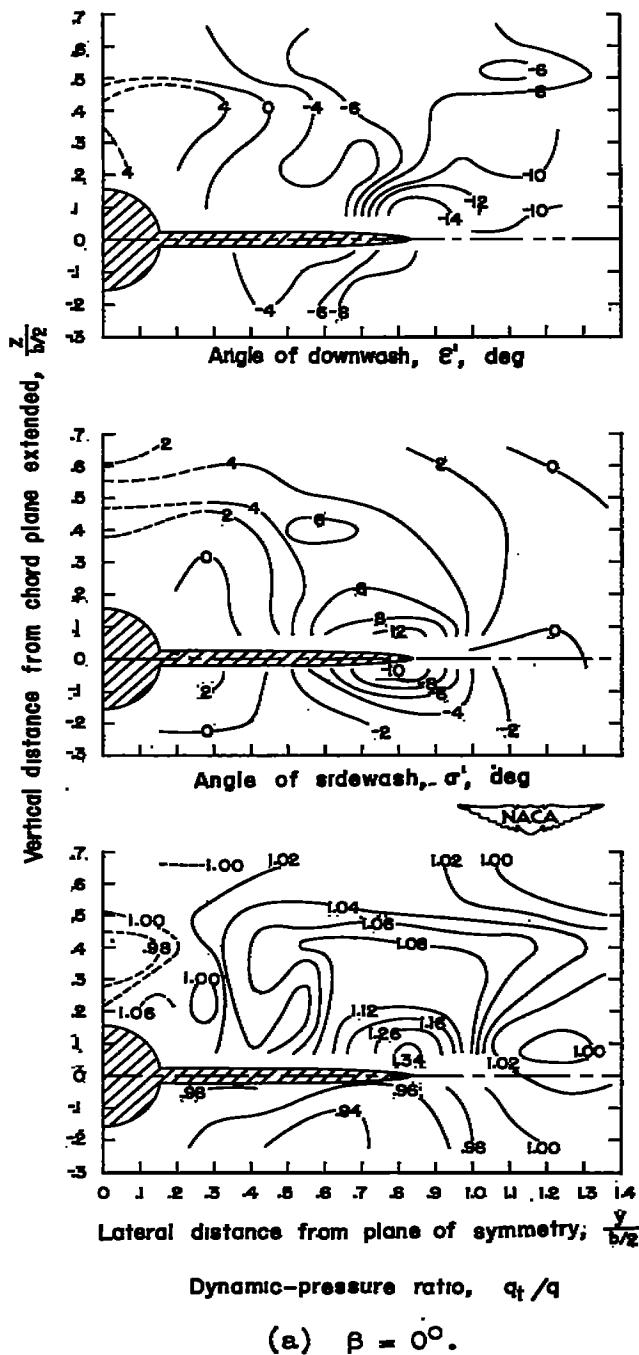
(a) $\beta = 0°$.

Figure 11.- Contour charts of downwash angle, sidewash angle, and dynamic-pressure ratio for a $60°$ delta-wing model. Plane of survey at $0.75\bar{c}$. $\delta_t = 0°$; $\alpha = 8.6°$; $C_L = 0.37$; $R = 9.0 \times 10^6$; configuration B.

Angle of downwash, ε', deg

Angle of sidewash, σ', deg

Lateral distance from plane of symmetry, $\frac{y}{b/2}$

Dynamic—pressure ratio, q_t/q

Vertical distance from chord plane extended, $\frac{z}{b/2}$

(b) $\beta = -3.5°$.

Figure 11.- Continued.

Angle of downwash, ε', deg

Angle of sidewash, σ', deg

Lateral distance from plane of symmetry, $\frac{y}{b/2}$

Dynamic-pressure ratio, q_t/q

Vertical distance from chord plane extended, $\frac{z}{b/2}$

(c) $\beta = -7°$.

Figure 11.- Concluded.

Angle of downwash, ε', deg

Angle of sidewash, σ', deg

Vertical distance from chord plane extended, $\frac{z}{b/2}$

Lateral distance from plane of symmetry, $\frac{y}{b/2}$

Dynamic-pressure ratio, q_t/q

(a)　$\beta = 0°$.

Figure 12.- Contour charts of downwash angle, sidewash angle, and dynamic-pressure ratio for a 60° delta-wing model. Plane of survey at 0.75$\bar{c}$. $\delta_t = 0°$; $\alpha = 25.7°$; $C_L = 1.15$; $R = 9.0 \times 10^6$; configuration B.

Angle of downwash, ε', deg

Angle of sidewash, σ', deg

Dynamic-pressure ratio, q_t/q

Lateral distance from plane of symmetry, $\frac{y}{b/2}$

Vertical distance from chord plane extended, $\frac{z}{b/2}$

(b) $\beta = -3.5^\circ$.

Figure 12.- Continued.

Angle of downwash, ε', deg

Angle of sidewash, σ', deg

Lateral distance from plane of symmetry, $\frac{y}{b/2}$

Dynamic-pressure ratio, q_t/q

Vertical distance from chord plane extended, $\frac{z}{b/2}$
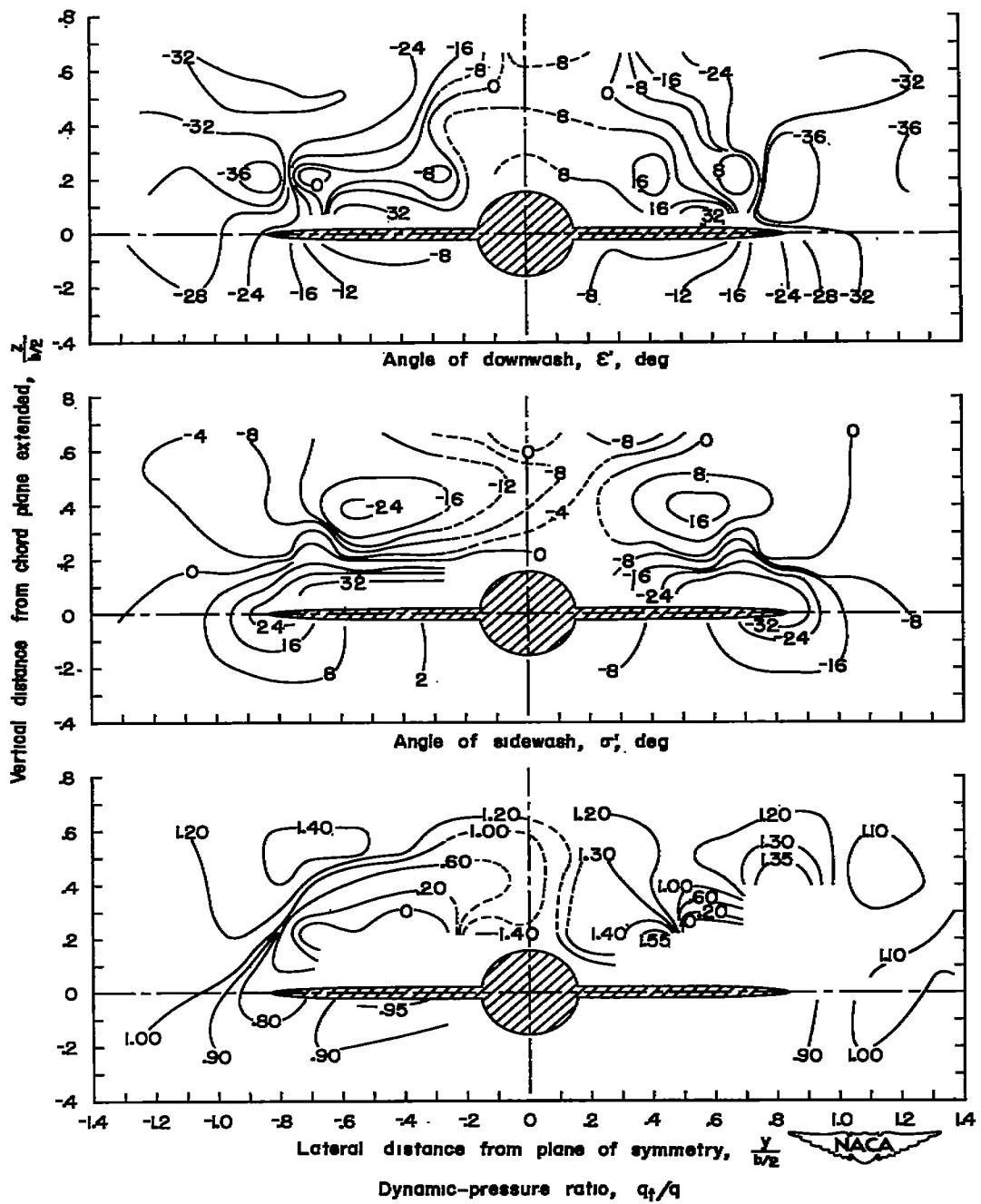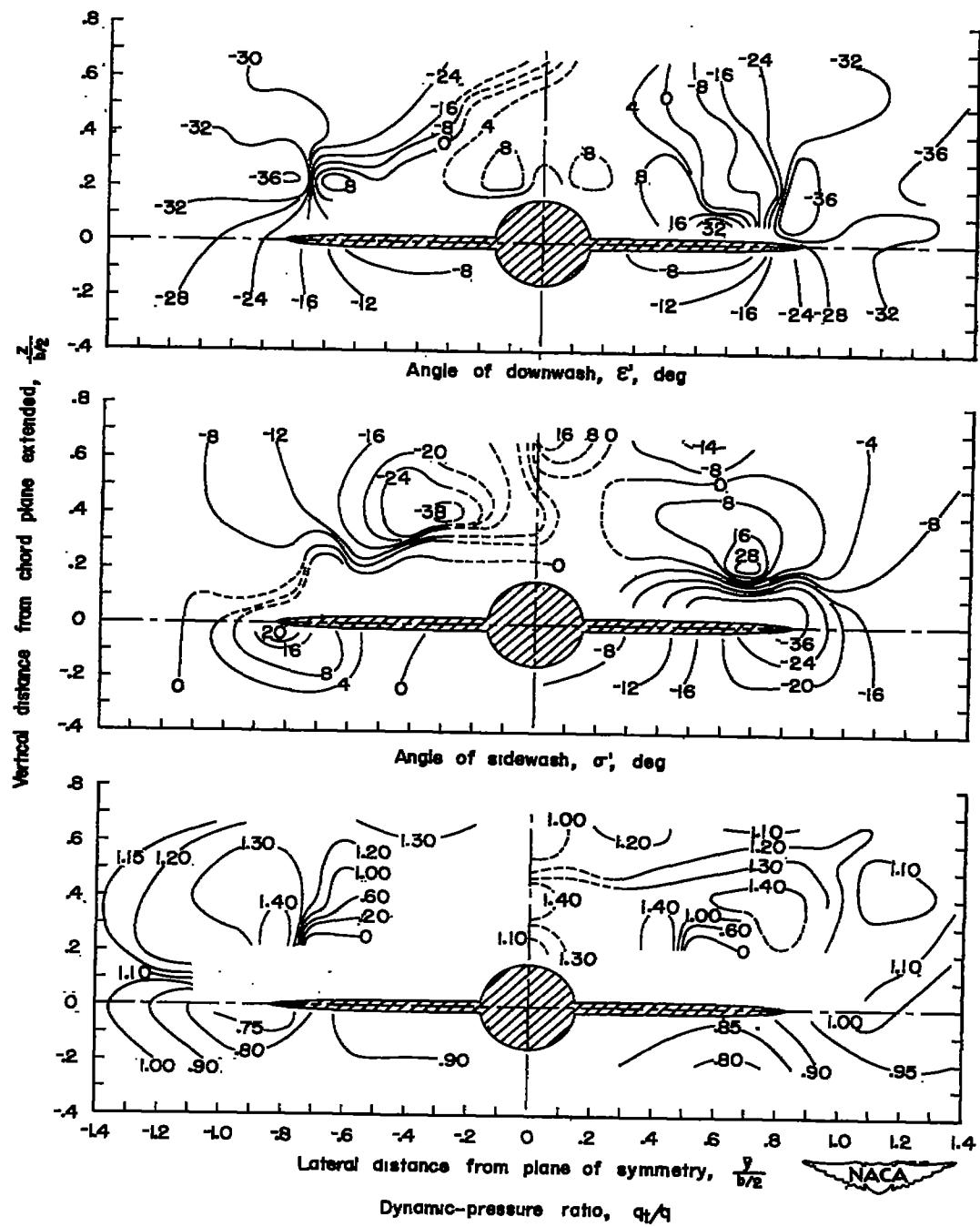
(c) $\beta = -7°$.

Figure 12.- Concluded.

(a) $\alpha = 8.6°$. (b) $\dot{\alpha} = 25.7°$.
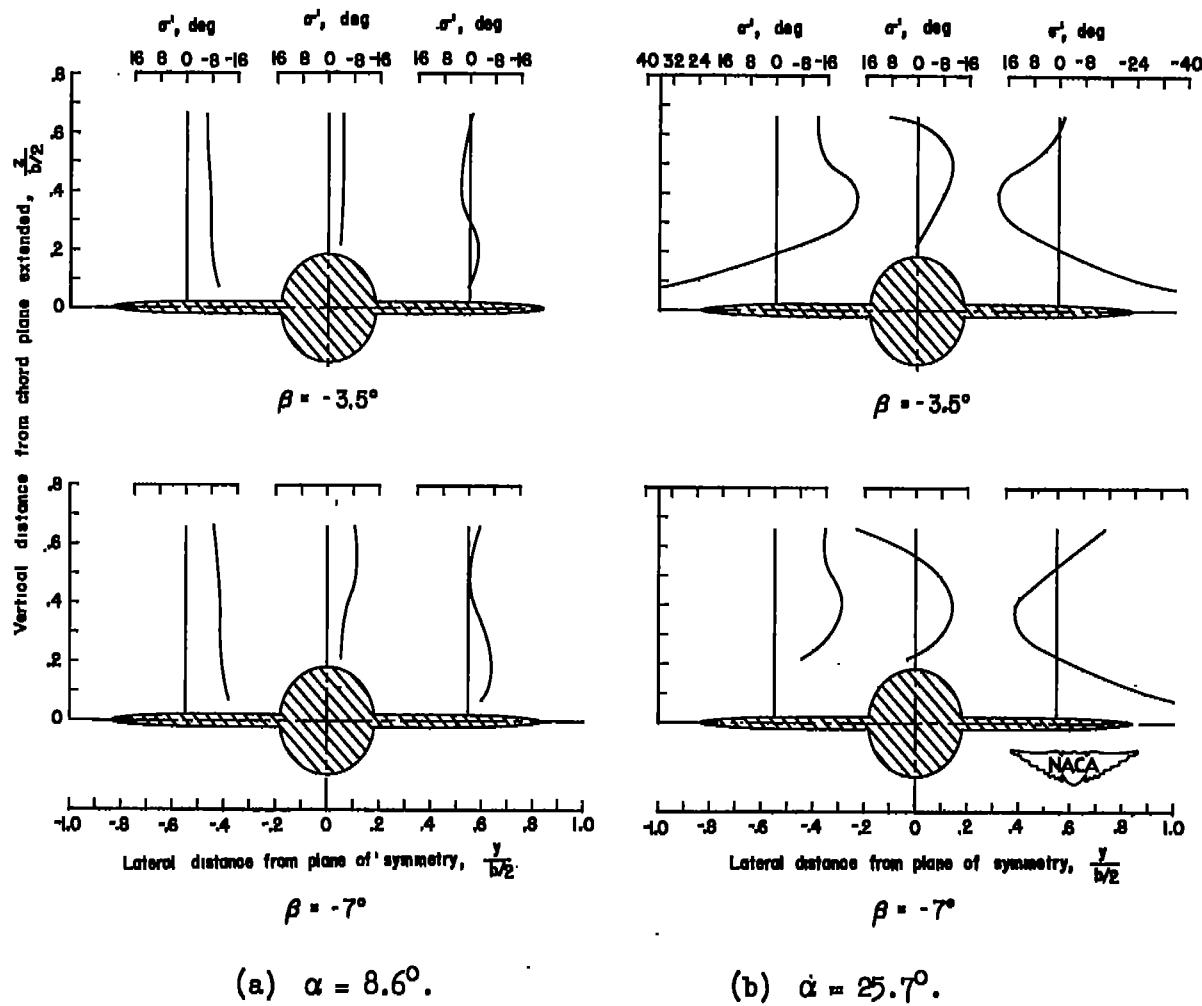
Figure 13.- Sidewash characteristics at central and outboard vertical fin locations for a 60° delta-wing—fuselage model with canard tail at various combinations of pitch and sideslip angles. Plane of survey at 0.75c̄.
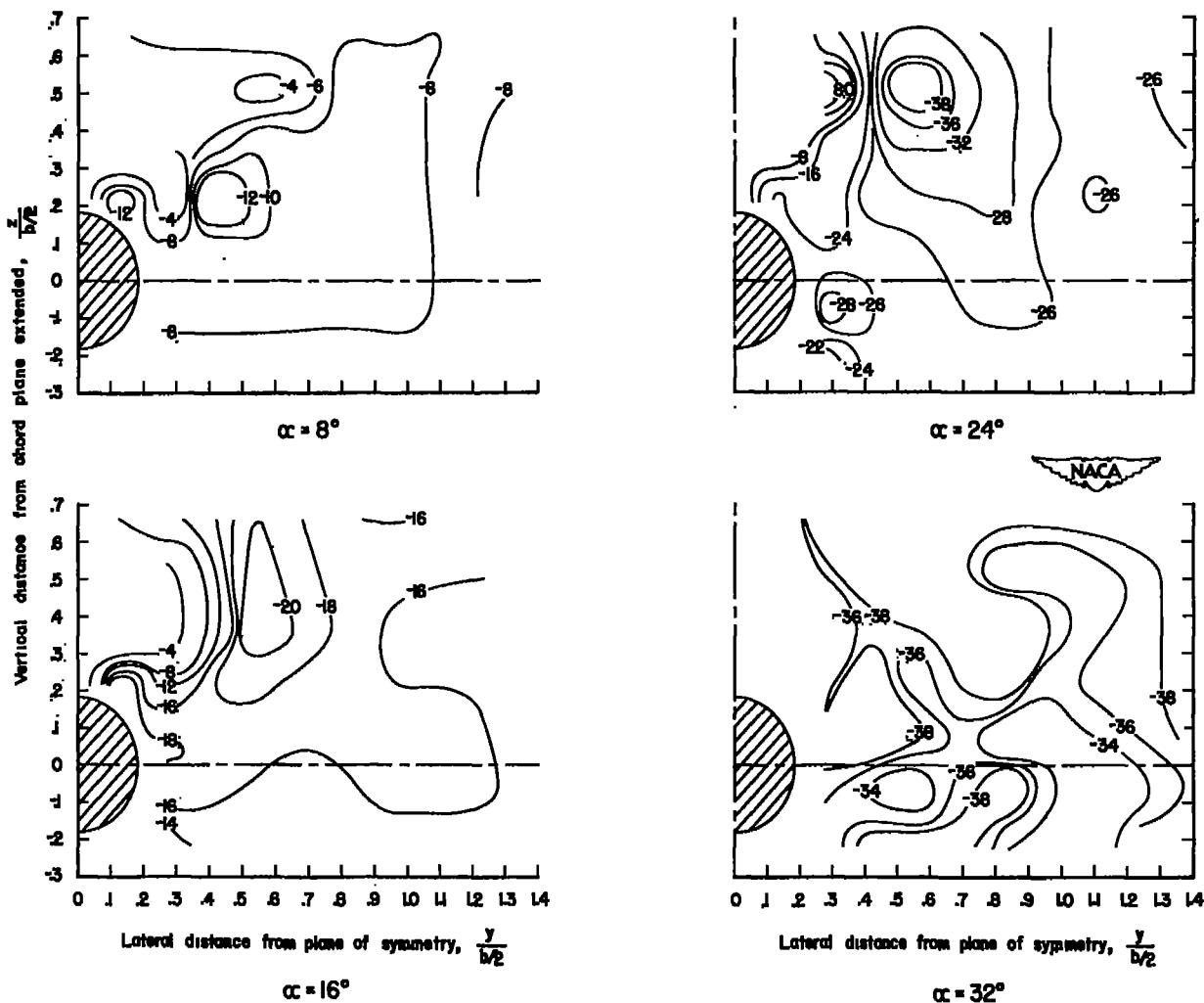
Figure 14.- Contour charts of downwash angle for a 60° delta wing mounted on a fuselage as a canard tail. Survey plane located 1.93c̄ behind nose of fuselage. β = 0°; δ_t = 0°; R = 9.0 x 10^6; configuration A.
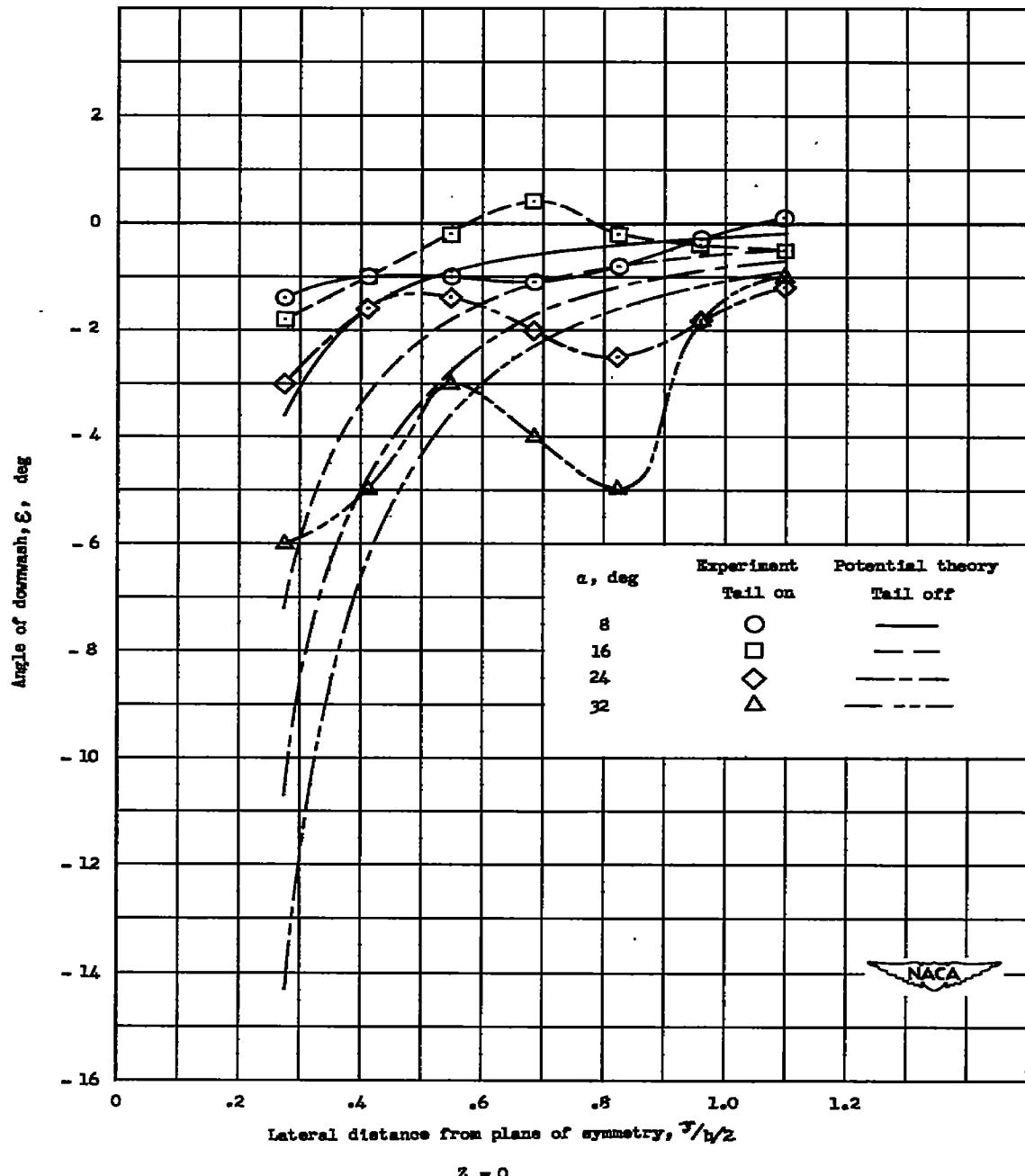
Figure 15.- Comparison of spanwise variation of experimental downwash
    angles for a canard tail in the presence of a fuselage with theoretical
   values of downwash for the fuselage alone.
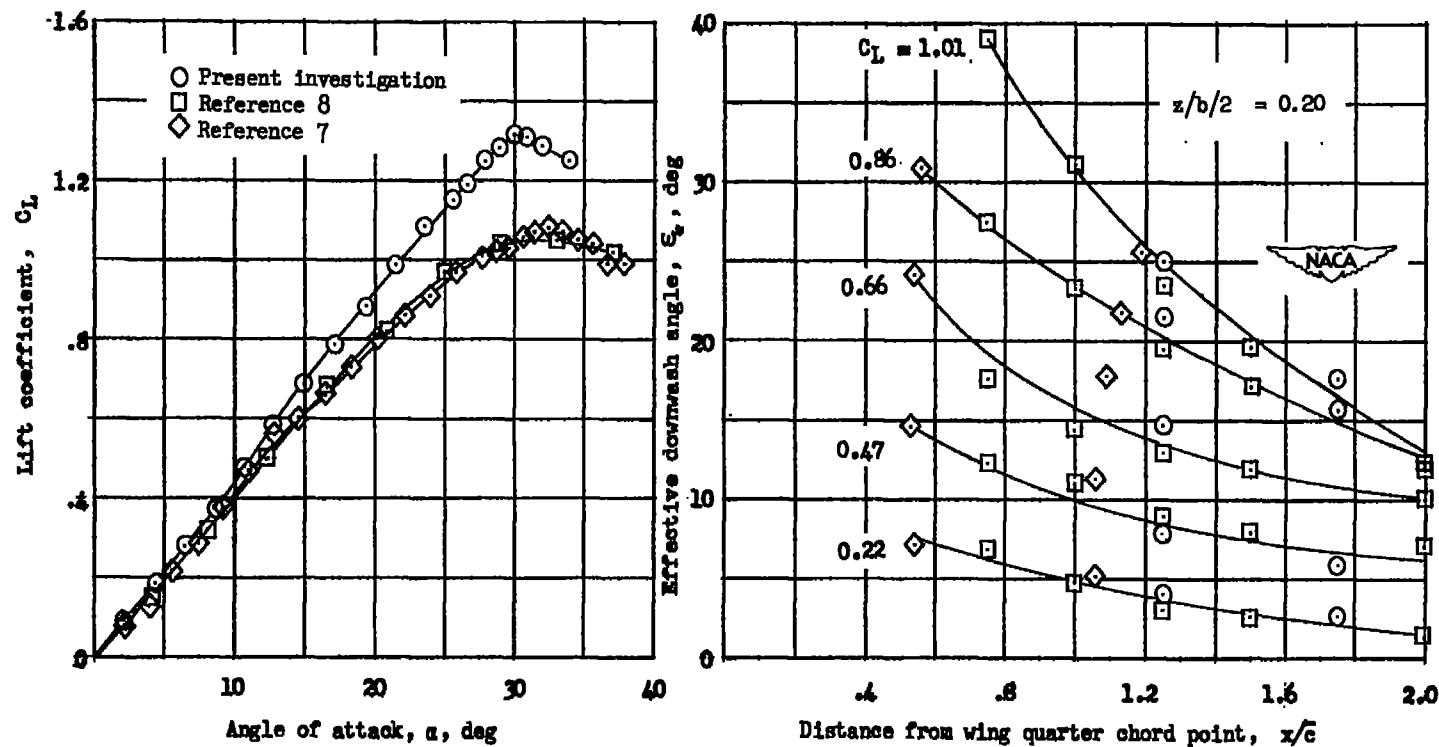
Figure 16.- Comparison of lift and effective downwash angles behind 60°
triangular wings from various sources.